

A MONOLITHIC hp SPACE-TIME MULTIGRID PRECONDITIONED NEWTON-KRYLOV SOLVER FOR SPACE-TIME FEM APPLIED TO THE INCOMPRESSIBLE NAVIER-STOKES EQUATIONS*

NILS MARGENBERG[†] AND MARKUS BAUSE[‡]

Abstract. We present a monolithic hp space-time multigrid method (hp -STMG) for tensor-product space-time finite element discretizations of the incompressible Navier–Stokes equations. We employ mapped inf-sup stable pairs $\mathbb{Q}_{r+1}/\mathbb{P}_r^{\text{disc}}$ in space and a slabwise discontinuous Galerkin DG(k) discretization in time. The resulting fully coupled nonlinear systems are solved by Newton–GMRES preconditioned with hp -STMG, combining geometric coarsening in space with polynomial coarsening in space and time. Our main contribution is an hp -robust and practically efficient extension of space-time multigrid to Navier–Stokes: matrix-free operator evaluation is retained via column-wise, state-dependent spatial kernels; the nonlinear convective term is handled by a reduced, order-preserving time quadrature. Robustness is ensured by an inexact space-time Vanka smoother based on patch models with single time point evaluation. The method is implemented in the matrix-free multigrid framework of **deal.II** and demonstrates h - and p -robust convergence with robust solver performance across a range of Reynolds numbers, as well as high throughput in large-scale MPI-parallel experiments with more than 10^{12} degrees of freedom.

Key words. Space-time finite elements, space-time multigrid, monolithic multigrid, matrix-free, higher-order finite elements, high-performance computing

MSC codes. 65M60, 65M55, 65F10, 65Y05

1. Introduction. Accurate and efficient simulation of incompressible flows remains challenging, particularly in the high-resolution, high-order regime. Space-time finite element methods (STFEMs) provide a natural framework for parallelism in space and time by treating time as an additional coordinate and enabling a unified variational discretization. This work transfers our space-time multigrid methodology for the instationary Stokes equations [21] to the nonlinear Navier–Stokes case. Two key ingredients make this extension feasible in a matrix-free setting: (i) a *tailored reduced time quadrature* for nonlinear space-time terms to reduce the cost per residual/Jacobian application while preserving the overall temporal order, and (ii) an *inexact* space-time Vanka smoother based on a coefficient patch model evaluated at a single time point, enabling reuse of local factorizations. We prove that lower-order quadrature for the nonlinear triple products preserves the discretization order, and that the inexact smoother remains uniformly close to the exact Vanka smoother. Numerically, this controlled inexactness does not degrade Newton–Krylov convergence or multigrid robustness.

We consider slab-wise tensor-product space-time discretizations. In space, we use mapped, inf-sup stable $\mathbb{Q}_{r+1}/\mathbb{P}_r^{\text{disc}}$ pairs with $r \in \mathbb{N}$, and in time a discontinuous Galerkin method DG(k) of order $k \in \mathbb{N}_0$. Continuous-in-time Galerkin discretizations are not pursued here, since a satisfactory definition of a continuous pressure trajectory remains an open issue; cf. [6]. The difficulty is that the initial pressure value is defined implicitly by the Navier–Stokes equations. The resulting nonlinear space-time system is solved by Newton–GMRES iterations preconditioned by an hp space-time multigrid method (hp STMG), combining geometric and polynomial coarsening in space and

*Submitted to the editors DATE.

[†]University of Magdeburg, Institute for Analysis and Numerics, Universitätsplatz 2, 39104 Magdeburg, Germany, nils.margenberg@ovgu.de

[‡]Helmut Schmidt University, Faculty of Mechanical and Civil Engineering, Holstenhofweg 85, 22043 Hamburg, Germany

time. Here, p -multigrid refers to coarsening in polynomial degree, while h -multigrid (geometric multigrid) refers to mesh coarsening. In our implementation, h -coarsening is restricted to space due to the time-marching realization; temporal h -coarsening is deferred to future work. Our implementation is based on the matrix-free multigrid framework in `deal.II` [2, 19, 24, 9]. The source code is available [20].

Matrix-free *monolithic* multigrid methods for Stokes-type systems are a prototypical building block for high-order incompressible flow solvers [18, 14]. Monolithic ph -multigrid preconditioners have been studied for high-order stationary Stokes [33]. Matrix-free Newton–Krylov solvers preconditioned by monolithic multigrid have also been demonstrated for stabilized incompressible Navier–Stokes [27], and high-order space-time DG formulations for incompressible Navier–Stokes are available [28]. Slabwise tensor-product space-time discretizations with Newton solvers have been investigated [29]. The present work targets robust, scalable hp multigrid preconditioning for nonlinear tensor-product space-time finite element Navier–Stokes systems.

Parallel-in-time integration methods address the sequential bottleneck of classical time stepping; see [10]. Fully implicit Runge–Kutta (FIRK) methods offer a complementary route to high-order time integration but lead to large coupled stage systems, closely related to tensor-product STFEM. Stage-parallel and transformed solvers for FIRK systems in DG-based flow simulations are developed in [25], and Vanka-based monolithic multigrid for implicit Runge–Kutta discretizations of incompressible flow is studied in [1]. Further developments for FIRK systems with nonlinearities and multilevel block solvers are addressed in [31, 23].

We retain the STFEM viewpoint and show that the space-time multigrid methodology developed in [21, 22] can be made practical for Navier–Stokes via temporal underintegration and an inexact space-time Vanka smoother. The choice of the smoother is motivated by the proven effectiveness of Vanka-type smoothers in fluid mechanics [3, 4, 21], coupled multiphysics [8, 5] and acoustic wave equations [22].

This paper is organized as follows. Section 2 introduces the continuous problem and the space-time finite element discretization. The resulting nonlinear algebraic system is derived in Section 3. Section 4 presents the hp -STMG preconditioned Newton–GMRES solver used throughout. Numerical experiments are reported in Section 5. Section 6 concludes with an evaluation of the results and an outlook.

2. Continuous and discrete problem.

2.1. Continuous problem. We consider the incompressible, nonstationary Navier–Stokes system

$$\begin{aligned}
 (2.1a) \quad & \partial_t \mathbf{v} + (\mathbf{v} \cdot \nabla) \mathbf{v} - \nu \Delta \mathbf{v} + \nabla p = \mathbf{f} & \text{in } \Omega \times (0, T), \\
 (2.1b) \quad & \nabla \cdot \mathbf{v} = 0 & \text{in } \Omega \times (0, T), \\
 (2.1c) \quad & \mathbf{v}(0) = \mathbf{v}_0 & \text{in } \Omega, \\
 (2.1d) \quad & \mathbf{v} = \mathbf{g}_D & \text{on } \Gamma_D \times (0, T), \\
 (2.1e) \quad & (\nu \nabla \mathbf{v} - p \mathbf{I}) \mathbf{n} = \mathbf{0} & \text{on } \Gamma_N \times (0, T).
 \end{aligned}$$

Here, $\Omega \subset \mathbb{R}^d$, $d \in \{2, 3\}$, is a bounded Lipschitz domain and $T > 0$ the final time. We split $\Gamma := \partial\Omega$ into Γ_D and Γ_N , i.e. $\Gamma = \overline{\Gamma_D} \cup \overline{\Gamma_N}$, with $|\Gamma_D|_{d-1} > 0$, $|\Gamma_N|_{d-1} > 0$, and $\Gamma_D \cap \Gamma_N = \emptyset$. The outward unit normal of Γ is $\mathbf{n} = \mathbf{n}(\mathbf{x})$ and \mathbf{I} denotes the identity matrix. The unknowns in (2.1) are the velocity field \mathbf{v} and pressure p , while \mathbf{f} , \mathbf{g}_D , and \mathbf{v}_0 are given, sufficiently smooth data. The kinematic viscosity satisfies $\nu > 0$. We assume sufficient regularity of solutions to (2.1), in particular up to $t = 0$, to justify higher-order space-time approximations.

We use standard notation. $H^m(\Omega)$ denotes the Sobolev space of $L^2(\Omega)$ functions with (weak) derivatives up to order m in $L^2(\Omega)$. The $L^2(\Omega)$ inner product (and its vector- and tensor-valued counterparts) is denoted by $\langle \cdot, \cdot \rangle$, with boundary pairing $\langle \cdot, \cdot \rangle_\Gamma$ and $\Gamma \in \{\partial\Omega, \Gamma_D\}$. Further, we use $\partial_n \mathbf{w} := (\nabla \mathbf{w}) \mathbf{n}$. We define

$$\mathbf{V} := H^1(\Omega)^d, \quad Q := L^2(\Omega), \quad \mathbf{V}^{\text{div}} := \{\mathbf{v} \in \mathbf{V} \mid \langle \nabla \cdot \mathbf{v}, q \rangle = 0 \ \forall q \in Q\}.$$

Remark 2.1 (Non mixed-type boundary condition). If Dirichlet boundary conditions are prescribed on $\partial\Omega$ only, i.e. $\partial\Omega = \Gamma_D$, the pressure variable is determined uniquely up to a constant $c \in \mathbb{R}$ only. In this case, the pressure space is chosen as $Q(\Omega) := L^2(\Omega)$ with $L_0^2(\Omega) := \{q \in L^2(\Omega) \mid \int_\Omega q \, dx = 0\}$ instead of $L^2(\Omega)$ such that its uniqueness is ensured. Further, we refer to [21] for the modifications that have to be made for $\Gamma = \Gamma_D$ in the construction of the multigrid method.

For the weak formulation of (2.1), let $\mathbf{X} := \mathbf{V} \times Q$. The semilinear form $A : \mathbf{X} \times \mathbf{X} \rightarrow \mathbb{R}$ with convective form of the first-order term in (2.1a) is given by

$$(2.2) \quad A(\mathbf{u})(\mathbf{w}) := \langle (\mathbf{v} \cdot \nabla) \mathbf{v}, \mathbf{z} \rangle + \langle \nu \nabla \mathbf{v} - p \mathbf{I}, \nabla \mathbf{z} \rangle + \langle \nabla \cdot \mathbf{v}, q \rangle$$

for $\mathbf{u}, \mathbf{w} \in \mathbf{X}$, with $\mathbf{u} = (\mathbf{v}, p)$ and $\mathbf{w} = (\mathbf{z}, q)$. Well-definedness of A on $\mathbf{X} \times \mathbf{X}$ is ensured. For our unified tensor product approach, we rewrite the convective term by using that $(\mathbf{v} \cdot \nabla) \mathbf{v} = \nabla \cdot (\mathbf{v} \otimes \mathbf{v})$, if $\nabla \cdot \mathbf{v} = 0$. The tensor product of two vectors $\mathbf{a}, \mathbf{b} \in \mathbb{R}^d$ is defined by $\mathbf{a} \otimes \mathbf{b} = \mathbf{a} \mathbf{b}^\top$. This semilinear form $A^{tp} : \mathbf{X} \times \mathbf{X} \rightarrow \mathbb{R}$ with the convective term in divergence form is then given by

$$(2.3) \quad A^{tp}(\mathbf{u})(\mathbf{w}) := \langle \nu \nabla \mathbf{v} - p \mathbf{I} - \mathbf{v} \otimes \mathbf{v}, \nabla \mathbf{z} \rangle + \langle \nabla \cdot \mathbf{v}, q \rangle$$

for $\mathbf{u}, \mathbf{w} \in \mathbf{X}$. Well-definedness of (2.3) is ensured. The semilinear forms comprise volume integrals only. Boundary integrals from integration by parts are added below.

2.2. Space-time finite element discretization. The construction principle for the space-time finite element spaces explores the so-called tensor product of Hilbert spaces. It can be rooted on the concept of multi-linear forms of Hilbert spaces. The product form of the space-time finite element spaces is strongly exploited in the construction and efficient implementation of our multigrid preconditioner.

Time mesh and spaces. Let $I := (0, T]$ be partitioned into N subintervals $I_n := (t_{n-1}, t_n]$, $n = 1, \dots, N$, where $\tau = \max\{\tau_n \mid N = 1, \dots, N\}$. We denote the time mesh by $\mathcal{M}_\tau := \{I_1, \dots, I_N\}$. For $k \in \mathbb{N}_0$, let $\mathbb{P}_k(J; \mathbb{R})$ be the space of piece-wise polynomials with maximum degree k on $J \subset I$. We put

$$(2.4) \quad Y_\tau^k(I) := \{w_\tau : I \rightarrow \mathbb{R} \mid (w_\tau)|_{I_n} \in \mathbb{P}_k(I_n; \mathbb{R}) \ \forall I_n \in \mathcal{M}_\tau\}.$$

Spatial mesh and spaces. Let \mathcal{T}_h be a shape-regular quadrilateral/hexahedral mesh of Ω with mesh size $h > 0$. On $K \in \mathcal{T}_h$ we put, for fixed $r \in \mathbb{N}$,

$$(2.5) \quad \mathbf{V}^{r+1}(K) := (\mathbb{Q}_{r+1})^d \circ \mathbf{T}_K^{-1}, \quad Q^r(K) := \mathbb{P}_r^{\text{disc}} \circ \mathbf{T}_K^{-1},$$

where \mathbf{T}_K is the standard multilinear map from the reference element to K . We employ the mapped variant of $\mathbb{P}_r^{\text{disc}}$ for geometric consistency on curved/non-affine meshes and improved conditioning of the algebraic systems. Using (2.5), we define

$$(2.6a) \quad \mathbf{V}_h^{r+1}(\Omega) := \{\mathbf{v}_h \in \mathbf{V} : (\mathbf{v}_h)|_K \in \mathbf{V}_{r+1}(K) \ \forall K \in \mathcal{T}_h\},$$

$$(2.6b) \quad Q_h^r(\Omega) := \{q_h \in Q : (q_h)|_K \in Q_r(K) \ \forall K \in \mathcal{T}_h\}.$$

The subspace of \mathbf{V}_h of discretely divergence-free functions is

$$(2.7) \quad \mathbf{V}_h^{\text{div}}(\Omega) := \{\mathbf{v}_h \in \mathbf{V}_h^{r+1}(\Omega) \mid \langle \nabla \cdot \mathbf{v}_h, q_h \rangle = 0 \ \forall q_h \in Q_h^r(\Omega)\}.$$

Space-time tensor product spaces. The global fully discrete spaces are the algebraic tensor products

$$(2.8) \quad \mathbf{H}_{\tau h}^{\mathbf{v}} := Y_{\tau}^k(I) \otimes \mathbf{V}_h^{r+1}(\Omega), \quad H_{\tau h}^p := Y_{\tau}^k(I) \otimes Q_h^r(\Omega), \quad \mathbf{X}_{\tau h}^{kr} := \mathbf{H}_{\tau h}^{\mathbf{v}} \times H_{\tau h}^p.$$

Remark 2.2 (Tensor products and Bochner spaces). The algebraic tensor product $Y_{\tau}(I) \otimes V_h(\Omega)$ is the span of separable functions $f \otimes g : (t, \mathbf{x}) \mapsto f(t)g(\mathbf{x})$ with $f \in Y_{\tau}(I)$ and $g \in V_h(\Omega)$; see [26, Section 1.2.3]. The Hilbert spaces in (2.8) are isometric to the Bochner spaces $Y_{\tau}^k(I; \mathbf{V}_h^{r+1}(\Omega))$ and $Y_{\tau}^k(I; Q_h^r(\Omega))$ of piece-wise polynomial functions with values in \mathbf{V}_h^{r+1} and Q_h^r , respectively; cf. [26, Prop. 1.2.28].

Right limits and jumps in time. For any piece-wise smooth $w : I \rightarrow B$ with respect to \mathcal{M}_{τ} (for instance, $w \in \mathbf{H}_{\tau h}^{\mathbf{v}}$), we define the right limit $w^+(t_n) := \lim_{t \rightarrow n+0} w(t)$, $0 \leq n < N$, and the jump $\llbracket w \rrbracket_n := w^+(t_n) - w(t_n)$.

Nitsche imposition on Γ_D . Instead of enforcing Dirichlet boundary conditions by the definition of the solution space, we apply Nitsche's method that imposes Dirichlet boundary conditions in a weak form. This offers appreciable advantages in the implementation of our framework. For this, let the positive and negative parts of $y \in \mathbb{R}$ be denoted by $y^{\oplus} := \frac{1}{2}(|y| + y)$ and $y^{\ominus} := \frac{1}{2}(|y| - y)$.

Firstly, we address the case in that the convective term is written as $(\mathbf{v} \cdot \nabla) \mathbf{v}$. This is done in order to develop our approach for the tensor product from of the convection term. For brevity, we put $\mathbf{X}_h^r := \mathbf{V}_h^{r+1}(\Omega) \times Q_h^r$. We let $\gamma_1 > 0$ and $\gamma_2 > 0$ denote two algorithmic parameters. Their choice is addressed below. The semilinear form $B_{\gamma} : \mathbf{V} \times \mathbf{X}_h \rightarrow \mathbb{R}$ is defined, for $\mathbf{v} \in \mathbf{V}$ and $\mathbf{w}_h \in \mathbf{X}_h$, by

$$(2.9a) \quad B_{\gamma}(\mathbf{v}, \mathbf{w}_h) := B^c(\mathbf{v}, \mathbf{w}_h) + B^s(\mathbf{v}, \mathbf{w}_h) + B_{\gamma}^r(\mathbf{v}, \mathbf{w}_h),$$

$$(2.9b) \quad B^c(\mathbf{v}, \mathbf{w}_h) := -\langle (\mathbf{v} \cdot \mathbf{n})^{\ominus} \mathbf{v}, \mathbf{z}_h \rangle_{\Gamma_D},$$

$$(2.9c) \quad B^s(\mathbf{v}, \mathbf{w}_h) := -\langle \mathbf{v}, (\nu \nabla \mathbf{z}_h + q_h \mathbf{I}) \mathbf{n} \rangle_{\Gamma_D}$$

$$(2.9d) \quad B_{\gamma}^r(\mathbf{v}, \mathbf{w}_h) := \nu \gamma_1 h_{\Gamma_D}^{-1} \langle \mathbf{v}, \mathbf{z}_h \rangle_{\Gamma_D} + \gamma_2 h_{\Gamma_D}^{-1} \langle \mathbf{v} \cdot \mathbf{n}, \mathbf{z}_h \cdot \mathbf{n} \rangle_{\Gamma_D}.$$

Along with (2.2), we let $A_{\gamma} : \mathbf{X}_h \times \mathbf{X}_h \rightarrow \mathbb{R}$, for $\mathbf{v}_h, \mathbf{w}_h \in \mathbf{X}_h$, be given by

$$(2.10) \quad A_{\gamma}(\mathbf{u}_h)(\mathbf{w}_h) := A(\mathbf{u}_h)(\mathbf{w}_h) - \langle (\nu \nabla \mathbf{v}_h - p_h \mathbf{I}) \mathbf{n}, \mathbf{z}_h \rangle_{\Gamma_D} + B_{\gamma}(\mathbf{v}_h, \mathbf{w}_h).$$

The terms (2.9) and (2.10) have the following explanations. The second term on the right hand side of (2.10) is due to the application of integration by parts and subtracts the natural boundary condition on Γ_D . The term in (2.9b) reflects the inflow boundary conditions. The term in (2.9c) is used to preserve the symmetry properties of the continuous system. The last two terms in (2.9d) are penalizations to ensure the stability of the discrete system. Together, the boundary pairings in (2.9) model the effective Dirichlet conditions in the three different flow regimes of viscous effects $\mathbf{v} = \mathbf{g}$, convective behavior $(\mathbf{v} \cdot \mathbf{n})^{\ominus} \mathbf{v} = (\mathbf{v} \cdot \mathbf{n})^{\ominus} \mathbf{g}$ and inviscid limit $(\mathbf{v} \cdot \mathbf{n} = \mathbf{g} \cdot \mathbf{n})$.

Next, we consider the divergence form $\nabla \cdot (\mathbf{v} \otimes \mathbf{v})$ of the convective term. Along with (2.2), we let $A_{\gamma}^{tp} : \mathbf{X}_h \times \mathbf{X}_h \rightarrow \mathbb{R}$, for $\mathbf{v}_h, \mathbf{w}_h \in \mathbf{X}_h$, be given by

$$(2.11) \quad \begin{aligned} A_{\gamma}^{tp}(\mathbf{u}_h)(\mathbf{w}_h) &:= A^{tp}(\mathbf{u}_h)(\mathbf{w}_h) - \langle (\nu \nabla \mathbf{v}_h - p_h \mathbf{I}) \mathbf{n}, \mathbf{z}_h \rangle_{\Gamma_D} \\ &\quad + \langle (\mathbf{v}_h \cdot \mathbf{n}) \mathbf{v}_h, \mathbf{z}_h \rangle_{\Gamma} + B_{\gamma}(\mathbf{v}_h, \mathbf{w}_h). \end{aligned}$$

The third term on the right-hand side of (2.11) is due to the application of integration by parts to the tensor product form of the convective term and ensures consistency.

In (2.11), we have with $y = y^\oplus - y^\ominus$ that

$$\begin{aligned} \langle (\mathbf{v}_h \cdot \mathbf{n}) \mathbf{v}_h, \mathbf{z}_h \rangle_\Gamma - \langle (\mathbf{v} \cdot \mathbf{n})^\ominus \mathbf{v}, \mathbf{z}_h \rangle_{\Gamma_D} \\ = \langle (\mathbf{v} \cdot \mathbf{n})^\oplus \mathbf{v}, \mathbf{z}_h \rangle_{\Gamma_D} - 2 \langle (\mathbf{v} \cdot \mathbf{n})^\ominus \mathbf{v}, \mathbf{z}_h \rangle_{\Gamma_D} + \langle (\mathbf{v} \cdot \mathbf{n}) \mathbf{v}, \mathbf{z}_h \rangle_{\Gamma_N}. \end{aligned}$$

In flow problems that are of interest in practice, the Dirichlet boundary portion Γ_D models an inflow boundary or fixed walls with no-slip condition. Then, $(\mathbf{v} \cdot \mathbf{n})^\oplus = 0$ is satisfied on Γ_D . Similarly, on the portion Γ_N the property $(\mathbf{v} \cdot \mathbf{n})^- = 0$ is satisfied. Together, this implies that

$$(2.12) \quad \langle (\mathbf{v}_h \cdot \mathbf{n}) \mathbf{v}_h, \mathbf{z}_h \rangle_\Gamma - \langle (\mathbf{v} \cdot \mathbf{n})^\ominus \mathbf{v}, \mathbf{z}_h \rangle_{\Gamma_D} = -2 \langle (\mathbf{v} \cdot \mathbf{n})^\ominus \mathbf{v}, \mathbf{z}_h \rangle_{\Gamma_D} + \langle (\mathbf{v} \cdot \mathbf{n})^\oplus \mathbf{v}, \mathbf{z}_h \rangle_{\Gamma_N}.$$

The terms on the right-hand side of (2.12) add further nonlinearities to the variational formulation. In the case of low Reynolds number flow, these quantities are small and might be neglected in computations. Further, for $\mathbf{z}_h = \mathbf{v}_h$ their nonnegativity is ensured, such that stability properties are not perturbed or weakened by the terms.

Fully discrete problem. We are now in a position to define our tensor-product space-time finite element approximation of the Navier–Stokes system (2.1). For the time discretization the discontinuous Galerkin method is applied.

Problem 2.3 (Discrete space-time variational problem). Let $\mathbf{f} \in L^2(I; \mathbf{H}^{-1}(\Omega))$ and $\mathbf{g}_D \in L^2(I; \mathbf{H}^{1/2}(\Gamma_D))$ be given. Let $\mathbf{v}_{0,h} \in \mathbf{V}_h^{\text{div}}(\Omega)$ denote an approximation of $\mathbf{v}_0 \in \mathbf{V}^{\text{div}}(\Omega)$. Find $\mathbf{u}_{\tau h} = (\mathbf{v}_{\tau h}, p_{\tau h}) \in \mathbf{X}_{\tau h}^{kr}$, with $\mathbf{v}_{\tau h}(0) := \mathbf{v}_{0,h}$, such that for all $\mathbf{w}_{\tau h} = (\mathbf{z}_{\tau h}, q_{\tau h}) \in \mathbf{X}_{\tau h}^{kr}$,

$$\begin{aligned} (2.13) \quad & \sum_{n=1}^N \int_{t_{n-1}}^{t_n} \langle \partial_t \mathbf{v}_{\tau h}, \mathbf{z}_{\tau h} \rangle + A_\gamma^{tp}(\mathbf{u}_{\tau h}, \mathbf{w}_{\tau h}) dt + \sum_{n=0}^{N-1} \langle [\mathbf{v}_{\tau h}]_n, \mathbf{z}_{\tau h}^+(t_n) \rangle \\ & = \sum_{n=1}^N \int_{t_{n-1}}^{t_n} \langle \mathbf{f}, \mathbf{z}_{\tau h} \rangle dt + \sum_{n=1}^N \int_{t_{n-1}}^{t_n} B_\gamma(\mathbf{g}, \mathbf{w}_{\tau h}) dt. \end{aligned}$$

Remark 2.4 (Preservation of tensor-product structure). In (2.13), all linear space-time terms can be written as algebraic tensor products of purely time and space dependent contributions; cf. Section 3. In contrast to the linear parts, the convective terms depend on the velocity itself. This destroys the strict separability of time and space. Nevertheless, the associated spatial operators can be built as algebraic tensor products, depending on the velocity as time dependent coefficient function. The contribution of the convective terms and their Jacobian matrices remain amenable to matrix-free, sum-factorized evaluation, cf. Subsection 4.4. For the construction of the matrix based smoother, we construct a separable surrogate by evaluating the convection field in the midpoint of I_n , which restores a Kronecker product structure inside the smoother without altering the outer FGMRES operator; cf. Subsection 4.3.

3. Algebraic system. Here, we derive the algebraic form of Problem 2.3 by exploiting the space-time tensor product structure (2.8) of the discrete spaces. The tensor product form is preserved in the algebraic system. This simplifies the assembly of the finite element matrices by factorizing into space and time integrals. The matrix-free framework becomes efficient. The treatment of the nonlinear convective term is more involved, but it can still be captured in this tensor product approach. An embedding of the Newton linearized, tensor product structured algebraic system into an hp multigrid preconditioning concept is developed in Subsection 4.2.

3.1. Preliminaries. For the evaluation of the time integrals in (2.13), we employ the right-sided $(k+1)$ -point Gauss-Radau quadrature on $I_n = (t_{n-1}, t_n]$,

$$(3.1) \quad Q_n(w) := \frac{\tau_n}{2} \sum_{\mu=1}^{k+1} \hat{\omega}_\mu w(t_n^\mu) \approx \int_{I_n} w(t) dt,$$

where $t_n^\mu = T_n(\hat{t}_\mu)$ with $T_n(\hat{t}) := (t_{n-1} + t_n)/2 + (\tau_n/2)\hat{t}$ and $\{\hat{t}_\mu, \hat{\omega}_\mu\}_{\mu=1}^{k+1}$ are the Gauss-Radau points and corresponding weights on $[-1, 1]$. The rule (3.1) is exact for all $w \in \mathbb{P}_{2k}(I_n; \mathbb{R})$ and $t_n^{k+1} = t_n$. Therefore, it is not exact for the nonlinear terms in (2.13). The quadrature error will be analyzed below in Lemma 3.2.

For the temporal finite element space (2.4), we use the local Lagrange basis associated with the Gauss-Radau nodes and supported on single subintervals I_n ,

$$(3.2) \quad \begin{aligned} Y_\tau^k(I) &= \text{span} \left\{ \varphi_n^a \in L^2(I) \mid (\varphi_n^a)|_{I_b} \in \mathbb{P}_k(I_b; \mathbb{R}), b = 1, \dots, N, \text{ supp } \varphi_n^a \subset \bar{I}_n, \right. \\ &\quad \left. \varphi_n^a(t_n^\mu) = \delta_{a,\mu}, \mu = 1, \dots, k+1, a = 1, \dots, k+1, n = 1, \dots, N \right\}, \end{aligned}$$

with the Kronecker symbol $\delta_{a,\mu}$. For the spatial discretization, we introduce the global finite element bases associated with the finite element spaces (2.6) by

$$(3.3) \quad \mathbf{V}_h^{r+1}(\Omega) = \text{span} \{ \boldsymbol{\chi}_m^{\mathbf{v}} \}_{m=1}^{M^{\mathbf{v}}}, \quad Q_h^r(\Omega) = \text{span} \{ \chi_m^p \}_{m=1}^{M^p}.$$

On each slab $\Omega \times I_n$, the tuple $(\mathbf{v}_{\tau h}, p_{\tau h}) \in \mathbf{H}_{\tau h}^{\mathbf{v}} \times H_{\tau h}^p$ has the tensor-product form

$$(3.4) \quad \mathbf{v}_{\tau h|I_n} = \sum_{a=1}^{k+1} \sum_{m=1}^{M^{\mathbf{v}}} v_n^{a,m} \varphi_n^a \boldsymbol{\chi}_m^{\mathbf{v}}, \quad p_{\tau h|I_n} = \sum_{a=1}^{k+1} \sum_{m=1}^{M^p} p_n^{a,m} \varphi_n^a \chi_m^p$$

with coefficients $v_n^{a,m} \in \mathbb{R}^d$ and $p_n^{a,m} \in \mathbb{R}$, for $a = 1, \dots, k+1$ and $m = 1, \dots, M$, with $M \in \{M^{\mathbf{v}}, M^p\}$. On each slab, we assemble the vectors of unknowns by

$$(3.5a) \quad \mathbf{V}_n^a := (v_n^{a,1}, \dots, v_n^{a,M^{\mathbf{v}}})^\top \in \mathbb{R}^{M^{\mathbf{v}}}, \quad \mathbf{P}_n^a := (p_n^{a,1}, \dots, p_n^{a,M^p})^\top \in \mathbb{R}^{M^p},$$

$$(3.5b) \quad \mathbf{V}_n := (\mathbf{V}_n^1, \dots, \mathbf{V}_n^{k+1})^\top \in \mathbb{R}^{(k+1)M^{\mathbf{v}}}, \quad \mathbf{P}_n := (\mathbf{P}_n^1, \dots, \mathbf{P}_n^{k+1})^\top \in \mathbb{R}^{(k+1)M^p}.$$

Assembly of the bilinear and linear terms in (2.13). The matrices assembled from the bilinear contributions in (2.13) for the tensor product spaces (2.8) and their bases in (3.2) and (3.3), respectively, are defined explicitly in Appendix A. The algebraic counterpart of the linear forms in (2.13) are summarized in Appendix A as well.

Assembly of the nonlinear convective terms in (2.13). For the tensor product framework, the treatment of the nonlinear convective terms in (2.13) contributing to A_γ^{tp} and B_γ is more involved. For the application of Newton's method to the nonlinear system, the Jacobian of the nonlinear contributions is needed further. This is derived in the sequel. We let $c: \mathbf{V}_h^{r+1} \times \mathbf{V}_h^{r+1} \rightarrow \mathbb{R}$ be defined by

$$(3.6) \quad c(\mathbf{v}_h)(\mathbf{z}_h) := -\langle \mathbf{v}_h \otimes \mathbf{v}_h, \nabla \mathbf{z}_h \rangle + \langle (\mathbf{v}_h \cdot \mathbf{n}) \mathbf{v}_h, \mathbf{z}_h \rangle_\Gamma$$

for $\mathbf{v}_h, \mathbf{z}_h \in \mathbf{V}_h^{r+1}$. Its Gateaux derivative at \mathbf{v}_h in the direction $\hat{\mathbf{v}}_h \in \mathbf{V}_h^{r+1}$ is

$$(3.7) \quad \begin{aligned} c'(\mathbf{v}_h)(\hat{\mathbf{v}}_h, \mathbf{z}_h) &= -\langle \hat{\mathbf{v}}_h \otimes \mathbf{v}_h, \nabla \mathbf{z}_h \rangle - \langle \mathbf{v}_h \otimes \hat{\mathbf{v}}_h, \nabla \mathbf{z}_h \rangle \\ &\quad + \langle (\hat{\mathbf{v}}_h \cdot \mathbf{n}) \mathbf{v}_h, \mathbf{z}_h \rangle_\Gamma + \langle (\mathbf{v}_h \cdot \mathbf{n}) \hat{\mathbf{v}}_h, \mathbf{z}_h \rangle_\Gamma, \quad \forall \mathbf{z}_h \in \mathbf{V}_h^{r+1}. \end{aligned}$$

For some $\mathbf{v}_h \in \mathbf{V}_h^{r+1}$, let $\mathbf{V} \in \mathbb{R}^{M^{\mathbf{v}}}$ denote the coefficient vector with respect to the representation of \mathbf{v}_h in the basis $\{\boldsymbol{\chi}_m^{\mathbf{v}}\}_{m=1}^{M^{\mathbf{v}}}$ of \mathbf{V}_h^{r+1} ; cf. (3.3). By means of (3.6), we let $\mathbf{H}: \mathbb{R}^{M^{\mathbf{v}}} \rightarrow \mathbb{R}^{M^{\mathbf{v}}}$, $\mathbf{V} \mapsto H(\mathbf{V})$, with $\mathbf{v}_h = \sum_{m=1}^{M^{\mathbf{v}}} V_m \boldsymbol{\chi}_m^{\mathbf{v}} \in \mathbf{V}_h^{r+1}$, be given by

$$(3.8) \quad (\mathbf{H}(\mathbf{V}))_m := c(\mathbf{v}_h)(\boldsymbol{\chi}_m^{\mathbf{v}})$$

for $m = 1, \dots, M^v$. For some time slab vector $\mathbf{V}_n = (\mathbf{V}_n^1, \dots, \mathbf{V}_n^{k+1})^\top \in \mathbb{R}^{(k+1) \cdot M^v}$, we let $\mathbf{H} : \mathbb{R}^{(k+1) \cdot M^v} \rightarrow \mathbb{R}^{(k+1) \cdot M^v}$, $\mathbf{V} \mapsto H(\mathbf{V})$ be given by

$$(3.9) \quad \mathbf{H}_n(\mathbf{V}_n) := (\mathbf{H}(\mathbf{V}_n^1), \dots, \mathbf{H}(\mathbf{V}_n^{k+1}))^\top.$$

Using (3.1) for the basis of (3.2), it follows that

$$(3.10) \quad \sum_{b,c=1}^{k+1} \int_{I_n} \varphi_n^b(t) \varphi_n^c(t) \varphi_n^a(t) dt \approx \frac{\tau_n}{2} \sum_{\mu=1}^{k+1} \hat{\omega}_\mu \varphi_n^b(t_n^\mu) \varphi_n^c(t_n^\mu) \varphi_n^a(t_n^\mu),$$

for $a, b, c \in \{1, \dots, k+1\}$. We note that (3.10) does not amount to an identity since (3.2) is exact for all polynomials of order less or equal than $2k$ only, and $\varphi_n^b(t) \varphi_n^c(t) \varphi_n^a(t) \in \mathbb{P}_{3k}(I_n)$. The quadrature error in (3.10) is analyzed below in Subsection 3.2. From (3.10), we conclude that, with a quadrature error \mathbf{E}_c^{GR} ,

$$(3.11) \quad \left(\left(\int_{I_n} c(\mathbf{v}_{\tau,h}) (\varphi_n^a \chi_m^v) dt \right)_{m=1}^{M^v} \right)_{a=1}^{k+1} = (\mathbf{M}_n^\tau \otimes \mathbf{I}) \mathbf{H}_n(\mathbf{V}_n) + \mathbf{E}_c^{\text{GR}},$$

where $\mathbf{M}_n^\tau \in \mathbb{R}^{k+1, k+1}$ is diagonal and defined in (A.1a). The tensor (or right Kronecker) product $\mathbf{A} \otimes \mathbf{B}$ of $\mathbf{A} \in \mathbb{R}^{r,r}$ and $\mathbf{B} \in \mathbb{R}^{s,s}$, for $r, s \in \mathbb{N}$, is given by

$$(3.12) \quad \mathbf{A} \otimes \mathbf{B} := (a_{ij} \mathbf{B})_{i,j=1}^r.$$

Remark 3.1. The contributions to (2.13) that arise from the boundary pairings with the convective term in (2.9b) and (2.11) are assembled similarly to (3.11) as $(\mathbf{M}_n^\tau \otimes \mathbf{I}) \mathbf{N}_{\Gamma_D}^{\mathbf{v},c}(\mathbf{V}_n)$.

For solving the nonlinear algebraic system we apply Newton's method. For this, the Jacobian of the nonlinear mapping \mathbf{H}_n in (3.9) is needed. Recalling (3.7) or, alternatively, building the derivative of the mapping \mathbf{H} in (3.8) with respect to the unknown vector \mathbf{V} , we get the mapping $\mathbf{H}' : \mathbb{R}^{M^v} \rightarrow \mathbb{R}^{M^v, M^v}$, $\mathbf{V} \mapsto \mathbf{H}'(\mathbf{V})$ with

$$(3.13) \quad (\mathbf{H}'(\mathbf{V}))_{ms} = \frac{\partial H_m}{\partial V_s} = c'(\mathbf{v}_h)(\chi_s^v, \chi_m^v)$$

for $m, s = 1, \dots, M^v$. The Jacobian of \mathbf{H}_n in (3.9) is then computed as $\mathbf{H}'_n : \mathbb{R}^{(k+1) \cdot M^v} \rightarrow \mathbb{R}^{(k+1) \cdot M^v, (k+1) \cdot M^v}$, $\mathbf{V}_n \mapsto \mathbf{H}'_n(\mathbf{V})$ with the block diagonal structure

$$(3.14) \quad (\mathbf{H}'_n(\mathbf{V}_n)) = \text{diag}(\mathbf{H}'(\mathbf{V}_n^1), \dots, \mathbf{H}'(\mathbf{V}_n^{k+1})).$$

3.2. Temporal quadrature approximation of the nonlinear term. Here we analyze briefly the consistency error \mathbf{E}_c^{GR} in (3.11). It occurs if the convective term in (2.13), that is a polynomial of order $3k$ in time, is integrated in time by the Gauss–Radau quadrature formula (3.1), that is exact for all polynomials of order less or equal than $2k$ only. We present an error estimate for the time integration of the convective term that holds under suitable stability assumptions about the fully discrete solution. Rigorous error estimates for the overall scheme are beyond the scope of interest in this paper. The convergence behavior of our scheme is illustrated numerically in Section 5. This further illustrates that the approach is methodologically sound.

LEMMA 3.2 (Gauss–Radau quadrature error for divergence-form of convection). *For $k \in \mathbb{N}_0$, suppose that $\mathbf{u}_{\tau h} \in Y_{\tau}^k(I) \otimes \mathbf{V}_h^{\text{div}}$ satisfies, for $l = 0, \dots, k$,*

$$(3.15) \quad \max_{n=1, \dots, N} \left\{ \|\partial_t^l \mathbf{u}_{\tau h}\|_{L^\infty(I_n; \mathbf{H}^1(\Omega))} + \|\tilde{\Delta}_h \partial_t^l \mathbf{u}_{\tau h}\|_{L^\infty(I_n; \mathbf{L}^2(\Omega))} \right\} \leq A_k,$$

where $\tilde{\Delta}_h$ denotes the discrete Stokes operator (cf. [12, p. 297]), and A_k is independent of the mesh sizes τ_n and h . For $\mathbf{w}_{\tau h} \in Y_{\tau}^k(I) \otimes \mathbf{V}_h^{r+1}$ let

$$\mathcal{C}_n(\mathbf{u}_{\tau h})(\mathbf{w}_{\tau h}) := \int_{I_n} c(\mathbf{u}_{\tau h}(t))(\mathbf{w}_{\tau h}(t)) \, dt.$$

For the $(k+1)$ -point Gauss–Radau formula (3.1), we put

$$\mathcal{C}_n^{\text{GR}}(\mathbf{u}_{\tau h})(\mathbf{w}_{\tau h}) := \sum_{\mu=1}^{k+1} w_{n,\mu} c(\mathbf{u}_{\tau h}(t_n^\mu))(\mathbf{w}_{\tau h}(t_n^\mu)).$$

There exists a constant $B_k = B_k(A_k)$ such that there holds that

$$(3.16) \quad \left| \sum_{n=1}^N \left(\mathcal{C}_n(\mathbf{u}_{\tau h})(\mathbf{w}_{\tau h}) - \mathcal{C}_n^{\text{GR}}(\mathbf{u}_{\tau h})(\mathbf{w}_{\tau h}) \right) \right| \leq B_k \tau^{2k+1} \|\mathbf{w}_{\tau h}\|_{L^2(I; \mathbf{H}^1(\Omega))}.$$

Proof. For given $\mathbf{u}_{\tau h} \in Y_{\tau}^k(I) \otimes \mathbf{V}_h^{\text{div}}$ and $\mathbf{w}_{\tau h} \in Y_{\tau}^k(I) \otimes \mathbf{V}_h^{r+1}$, we have that $c(\mathbf{u}_{\tau h})(\mathbf{w}_{\tau h}) \in \mathbb{P}_{3k}(I_n; \mathbb{R})$. Since the Gauss–Radau quadrature formula is exact for polynomials in $\mathbb{P}_{2k}(I_n; \mathbb{R})$, the Peano kernel remainder yields that

$$(3.17) \quad \begin{aligned} E_n^{\text{GR}} &:= \mathcal{C}_n^{\text{GR}}(\mathbf{u}_{\tau h})(\mathbf{w}_{\tau h}) - \mathcal{C}_n^{\text{GR}}(\mathbf{u}_{\tau h})(\mathbf{w}_{\tau h}) \\ &= \kappa_k \tau_n^{2k+2} \partial_t^{2k+2} c(\mathbf{u}_{\tau h}(\xi_n))(\mathbf{w}_{\tau h}(\xi_n)) \\ &= \kappa_k \tau_n^{2k+2} \sum_{\substack{|\alpha| \leq 2k+2 \\ \alpha_i \leq k, i \in \{1, 2, 3\}}} c(\partial_t^{(\alpha_1, \alpha_2)} \mathbf{u}_{\tau h}(\xi_n))(\partial_t^{\alpha_3} \mathbf{w}_{\tau h}(\xi_n)) \end{aligned}$$

for some $\xi_n \in I_n$, with κ_k depending only on k . Here, the multiindex (α_1, α_2) denotes the respective order of the time derivative in the product of $\mathbf{u}_{\tau h}$ with itself in (3.6), i.e., $\partial_t^{(\alpha_1, \alpha_2)}(\mathbf{u}_{\tau h} \otimes \mathbf{u}_{\tau h}) := \partial_t^{\alpha_1} \mathbf{u}_{\tau h} \otimes \partial_t^{\alpha_2} \mathbf{u}_{\tau h}$. We recall that $\mathbf{u}_{\tau h}, \mathbf{w}_{\tau h} \in Y_{\tau}^k(I) \otimes \mathbf{V}_h^{r+1}$, such that their time derivatives of order $k+1$ or higher vanish.

Now, let $\mathbf{u}_h \in \mathbf{V}_h^{\text{div}}$, $\mathbf{w}_h \in \mathbf{V}_h^{r+1}$ be given. Recalling (3.6), there holds by the Hölder inequality and embedding theorems for the volume integrals and by [12, Eq. (4.46)] for the boundary terms that

$$(3.18) \quad |c(\mathbf{u}_h)(\mathbf{w}_h)| \leq c(\|\nabla \mathbf{u}_h\|^2 \|\nabla \mathbf{w}_h\| + \|\tilde{\Delta}_h \mathbf{u}_h\|^{1/2} \|\nabla \mathbf{u}_h\|^{1/2} (\|\mathbf{w}_h\| + h \|\nabla \mathbf{w}_h\|)).$$

Summing up (3.17) from $n = 1$ to N and using (3.18) along with (3.15) yields that

$$(3.19) \quad \left| \sum_{n=1}^N E_n^{\text{GR}} \right| \leq B_k \sum_{n=1}^N \tau_n^{2k+2} \sum_{l=0}^k \|\partial_t^l \mathbf{w}_{\tau h}\|_{L^\infty(I_n; \mathbf{H}^1(\Omega))}.$$

By the L^∞ – L^2 inverse property [17, Eq. (2.5)]

$$\|y\|_{L^\infty(I_n; \mathbb{R})} \leq c \tau_n^{-1/2} \|y\|_{L^2(I_n; \mathbb{R})}, \quad \text{for } y \in \mathbb{P}_k(I_n; \mathbb{R}),$$

and the H^1 – L^2 inverse property

$$\|\partial_t y\|_{L^2(I_n; \mathbb{R})} \leq c \tau_n^{-1} \|y\|_{L^2(I_n; \mathbb{R})}, \quad \text{for } y \in \mathbb{P}_k(I_n; \mathbb{R}),$$

we deduce from (3.19) that

$$(3.20) \quad \left| \sum_{n=1}^N E_n^{\text{GR}} \right| \leq B_k \sum_{n=1}^N \tau_n^{k+3/2} \|\mathbf{w}_{\tau h}\|_{L^2(I_n; \mathbf{H}^1(\Omega))}.$$

From (3.20), we conclude assertion (3.16) by the inequality of Cauchy–Schwarz. \square

Remark 3.3 (On the result of Lemma 3.2).

- The stability bounds in (3.15) are not straightforward. For the regularity of continuous and discrete solutions to the Navier–Stokes equations, the occurrence of non-local compatibility conditions, and uniform bounds up to $t = 0$, we refer to the comprehensive literature, in particular [12, 13].
- Inequality (3.16) yields an error estimation of the form as it is required and often applied in error analyses for Navier–Stokes approximations. After the additional application of the inequalities of Cauchy–Schwarz and Cauchy–Young and a suitable choice of the test function $\mathbf{w}_{\tau h}$, the term $\|\mathbf{w}_{\tau h}\|_{L^2(I; \mathbf{H}^1(\Omega))}$ can be absorbed by the viscous term of the error identity to the considered scheme; cp., e.g., [15].

3.3. Algebraic form of the discrete problem. Now, we rewrite Problem 2.3 in its algebraic form. By the choice of a local temporal basis in (3.2), supported on the subintervals I_n , we end up with a time marching scheme. In each time step, the nonlinear system of equations is solved by an inexact Newton–Krylov method using FGMRES iterations with hp multigrid preconditioning. Even if three space dimensions and higher order approximations are involved, the time marching approach is economical and becomes still feasible without tremendous computing power and memory resources. In contrast to this, a holistic approach solves the global in time nonlinear algebraic system; cf. Remark 3.5. In the Newton iteration, the block lower bi-diagonal structure of the global algebraic system can then be used for building a time marching process and splitting the global system into a sequence of local algebraic problems again. This approach is not studied here. We recast Problem 2.3, up to the quadrature error in the convective terms (cf. Subsection 3.2), in the following form.

Problem 3.4 (Local algebraic Navier–Stokes problem). Let $n \in \{1, \dots, N\}$. For $n > 1$ set $\mathbf{v}_{\tau h}(t_{n-1}) = \sum_{m=1}^{M^v} v_{n-1}^{k+1, m} \chi_m^v$, and for $n = 1$ set $\mathbf{v}_{\tau h}(t_0) = \mathbf{v}_{0, h} = \sum_{m=1}^{M^v} v_0^m \chi_m^v$. Define $\mathbf{V}_{n-1} \in \mathbb{R}^{(k+1) \cdot M^v}$ as

$$(3.21) \quad \mathbf{V}_{n-1} := \begin{cases} (\mathbf{0}, \dots, \mathbf{0}, v_{n-1}^{k+1, 1}, \dots, v_{n-1}^{k+1, M^v})^\top, & \text{for } n > 1, \\ (\mathbf{0}, \dots, \mathbf{0}, v_0^1, \dots, v_0^{M^v})^\top, & \text{for } n = 1. \end{cases}$$

Find $\mathbf{U}_n := (\mathbf{V}_n, \mathbf{P}_n) \in \mathbb{R}^{(k+1) \cdot (M^v + M^p)}$ such that

$$(3.22a) \quad \underbrace{(\mathbf{K}_n^\tau \otimes \mathbf{M}_h) \mathbf{V}_n}_{\text{time derivative}} + \underbrace{(\mathbf{M}_n^\tau \otimes \mathbf{I}) \mathbf{H}_n(\mathbf{V}_n)}_{\text{convection (divergence form)}} + \underbrace{(\mathbf{M}_n^\tau \otimes \nu \mathbf{A}_h) \mathbf{V}_n}_{\text{viscous}} + \underbrace{(\mathbf{M}_n^\tau \otimes \mathbf{B}_h^\top) \mathbf{P}_n}_{\text{pressure coupling}} + \underbrace{(\mathbf{M}_n^\tau \otimes \mathbf{I}) \mathbf{N}_{\Gamma_D}^{\mathbf{v}, c}(\mathbf{V}_n)}_{\substack{\text{Boundary pairings with} \\ \text{convective term in (2.11)}}} + \underbrace{(\mathbf{M}_n^\tau \otimes \mathbf{N}_{\Gamma_D}^{\mathbf{v}, b, r}(\gamma)) \mathbf{V}_n}_{\substack{\text{boundary condition and} \\ \text{Nitsche's term } B^s + B_\gamma^r \text{ in (2.11)}}} + \underbrace{(\mathbf{M}_n^\tau \otimes (\mathbf{G}_{\Gamma_D}^p)^\top) \mathbf{P}_n}_{\text{boundary condition}} = \underbrace{\mathbf{F}_n}_{\text{body force}} + \underbrace{\mathbf{L}_n}_{\substack{\text{Dirichlet data} \\ \text{via Nitsche}}} + \underbrace{(\mathbf{C}_n^\tau \otimes \mathbf{M}_h) \mathbf{V}_{n-1}}_{\substack{\text{jump at } t_{n-1} \text{ of DG in time}}},$$

$$(3.22b) \quad \underbrace{(\mathbf{M}_n^\tau \otimes \mathbf{B}_h) \mathbf{V}_n}_{\text{continuity}} + \underbrace{(\mathbf{M}_n^\tau \otimes \mathbf{G}_{\Gamma_D}^p) \mathbf{V}_n}_{\substack{\text{Nitsche's term } B^s \text{ in (2.11)}}} = \mathbf{0}.$$

On I_n , $\mathbf{u}_{\tau h} \in \mathbf{X}_{\tau h}^{kr}$ is then defined by the expansions in (3.4) along with (3.5). For the definition of the quantities in (3.22) we refer to Subsection 3.1 and Appendix A. Problem 3.4 leads to a global in time system with block lower bi-diagonal structure.

DEFINITION 3.5 (Global algebraic Navier–Stokes problem). *Suppose that \mathbf{V}_0 is given by (3.21). Find $\mathbf{U} := (\mathbf{U}_1, \dots, \mathbf{U}_n) \in \mathbb{R}^{N \cdot (k+1) \cdot (M^v + M^p)}$, such that*

$$(3.23) \quad \mathcal{R}(\mathbf{U}) = \mathbf{0}, \quad \text{with } \mathcal{R}(\mathbf{U}) \equiv \begin{pmatrix} \mathcal{R}_1(\mathbf{U}_1; \mathbf{V}_0) \\ \mathcal{R}_2(\mathbf{U}_2; \mathbf{V}_1) \\ \vdots \\ \mathcal{R}_N(\mathbf{U}_N; \mathbf{V}_{N-1}) \end{pmatrix},$$

with $\mathcal{R}_n : \mathbb{R}^{(k+1) \cdot (M^v + M^p)} \rightarrow \mathbb{R}^{(k+1) \cdot (M^v + M^p)}$, for $n = 1, \dots, N$, being defined by (3.22).

To solve the sequence of local in time problems (3.22), which amounts to solving (3.23) row-wise, we need the Jacobian matrix of the mapping in (3.22). It is given by

$$(3.24) \quad \mathcal{J}_n(\mathbf{U}_n) = \begin{pmatrix} \mathcal{J}_n^{1,1}(\mathbf{U}_n)_{1,1} & \mathcal{J}_n^{1,2}(\mathbf{U}_n) \\ \mathcal{J}_n^{2,1}(\mathbf{U}_n)_{2,1} & \mathcal{J}_n^{2,2}(\mathbf{U}_n) \end{pmatrix} \in \mathbb{R}^{(k+1) \cdot (M^v + M^p), (k+1) \cdot (M^v + M^p)},$$

with submatrices $\mathcal{J}_n^{1,1} \in \mathbb{R}^{(k+1) \cdot M^v, (k+1) \cdot M^v}$, $\mathcal{J}_n^{1,2} \in \mathbb{R}^{(k+1) \cdot M^v, (k+1) \cdot M^p}$ and $\mathcal{J}_n^{2,2} \in \mathbb{R}^{(k+1) \cdot M^p, (k+1) \cdot M^p}$ being defined by

$$(3.25a) \quad \mathcal{J}_n^{1,1}(\mathbf{U}_n) = \mathbf{K}_n^\tau \otimes \mathbf{M}_h + (\mathbf{M}_n^\tau \otimes \mathbf{I}) \mathbf{H}'_n(\mathbf{V}_n) + \mathbf{M}_n^\tau \otimes \nu \mathbf{A}_h \\ + (\mathbf{M}_n^\tau \otimes \mathbf{I})(\mathbf{N}_{\Gamma_D}^{\mathbf{v},c})'(\mathbf{V}_n) + \mathbf{M}_n^\tau \otimes \mathbf{N}_{\Gamma_D}^{\mathbf{v},b,r}(\gamma),$$

$$(3.25b) \quad \mathcal{J}_n^{1,2}(\mathbf{U}_n) = \mathbf{M}_n^\tau \otimes (\mathbf{B}_h + \mathbf{G}_{\Gamma_D}^p), \quad \mathcal{J}_n^{2,1}(\mathbf{U}_n) = \mathcal{J}_n^{1,2}(\mathbf{U}_n)^\top,$$

$$(3.25c) \quad \mathcal{J}_n^{2,2}(\mathbf{U}_n) = \mathbf{0}.$$

For this, we recall (3.14). We note that $(\mathbf{A} \otimes \mathbf{B})^\top = \mathbf{A}^\top \otimes \mathbf{B}^\top$ is satisfied. The matrix \mathbf{M}_n^τ is symmetric by its definition. By (3.25b), the Jacobian matrix has a saddle point structure. Moreover, a tensor product structure is preserved for its submatrices.

4. Solution of the nonlinear system of equations. We solve (3.22), recast in the system (3.23), by a Newton–Krylov method with FGMRES iterations and hp space-time multigrid preconditioning in a matrix-free framework. This is presented now in detail. The algorithms are summarized in Appendix B.

4.1. Inexact Newton–Krylov with Armijo globalization. We solve (3.23) row-wise. For this, we use Newton’s method with globalization by a nonmonotone Armijo rule [11]. We recall it briefly for completeness. Starting with some initial guess, suppose that the iterate $\mathbf{U}_n^m \in \mathbb{R}^{(k+1) \cdot (M^v + M^p)}$ has been computed. Then, we calculate the Newton correction $\widehat{\mathbf{U}}_n^m \in \mathbb{R}^{(k+1) \cdot (M^v + M^p)}$ by solving with the FGMRES method [30] the system

$$(4.1) \quad \mathcal{J}_n(\mathbf{U}_n^m) \widehat{\mathbf{U}}_n^m = -\mathcal{R}_n(\mathbf{U}_n^m; \mathbf{V}_{n-1}),$$

with the stopping criterion that

$$(4.2) \quad \|\mathcal{J}_n(\mathbf{U}_n^m) \widehat{\mathbf{U}}_n^m + \mathcal{R}_n(\mathbf{U}_n^m; \mathbf{V}_{n-1})\|_{\mathcal{M}} \leq \eta_m \|\mathcal{R}_n(\mathbf{U}_n^m; \mathbf{V}_{n-1})\|_{\mathcal{M}},$$

where the mass-weighted norm is defined by

$$\mathcal{M}_n := \begin{pmatrix} \mathbf{M}_n^\top \otimes \mathbf{M}_h & 0 \\ 0 & \mathbf{M}_n^\top \otimes \mathbf{M}_h^p \end{pmatrix}, \quad \|\mathbf{Z}\|_{\mathcal{M}_n} := (\mathbf{Z}^\top \mathcal{M}_n \mathbf{Z})^{1/2},$$

for $\mathbf{Z} = (\mathbf{Z}^v, \mathbf{Z}^p)$. For some $\eta_{\max}, c_{\text{EW}} \in (0, 1)$ and $\gamma_{\text{EW}} \in (1, 2]$, the parameter η_m is chosen as in [7]

$$(4.3) \quad \eta_m = \min \left\{ \eta_{\max}, c_{\text{EW}} \left(\frac{\|\mathcal{R}_n(\mathbf{U}_n^m; \mathbf{V}_{n-1})\|_{\mathcal{M}_n}}{\max\{\|\mathcal{R}_n(\mathbf{U}_n^{m-1}; \mathbf{V}_{n-1})\|_{\mathcal{M}_n}, \varepsilon\}} \right)^{\gamma_{\text{EW}}} \right\}.$$

Our globalization approach uses Armijo's backtracking with the merit function

$$\phi(\alpha) := \frac{1}{2} \|\mathcal{R}_n(\mathbf{U}_n^m + \alpha \widehat{\mathbf{U}}_n^m; \mathbf{V}_{n-1})\|_{\mathcal{M}}^2.$$

For $g_0 := \phi'(0) = \mathcal{R}_n(\mathbf{U}_n^m; \mathbf{V}_{n-1})^\top \mathcal{J}_n(\mathbf{U}_n^m) \widehat{\mathbf{U}}_n^m$ and the largest $\alpha \in (0, 1]$ such that

$$(4.4) \quad \phi(\alpha) \leq \phi(0) + c_1 \alpha g_0, \quad \text{for } c_1 \in (0, 1),$$

is satisfied, we then put

$$(4.5) \quad \mathbf{U}_n^{m+1} = \mathbf{U}_n^m + \alpha \widehat{\mathbf{U}}_n^m.$$

The Newton iteration along with its control is summarized in Algorithm 1 to 2.

4.2. Preconditioning of GMRES by hp space-time multigrid (STMG).

We solve (4.1) by FGMRES iterations [30] with right-sided hp space-time multigrid preconditioning. This approach was developed and analyzed in [21] for the linear Stokes problem. Geometric refinement and coarsening of the spatial and temporal mesh is referred to as h -multigrid, while the refinement and coarsening of the polynomial degree $k, r \in \mathbb{N}$ is referred to as p -multigrid. Here, h -multigrid is applied to the space variables only, since we solve (3.23) row-wise, which amounts to a time stepping process. In the sequel, we restrict ourselves to presenting only the differences to [21] and innovations of the preconditioner that are made for the nonlinear Navier–Stokes problem and the embedding of the FGMRES method into the Newton iterations. The preconditioner exploits the tensor product structure of the discrete solution space (2.8) and is implemented in a matrix-free form in the deal.II library [19] in order to enhance its efficiency. The FGMRES iterations for (4.1) are built on the evaluation of the Jacobian matrix computed in (3.24), whereas a surrogate of $\mathcal{J}_n(\cdot)$ is applied in the smoother of the STMG method (cf. Subsection 4.3). To present the STMG preconditioner, we need notation. For further details, we also refer to [21].

Multilevel hierarchies and discrete spaces. Let $\{\mathcal{T}_s\}_{s=0}^S$ be a quasi-uniform family of nested triangulations of the spatial domain Ω , with characteristic mesh sizes h_s satisfying $h_s \lesssim \frac{h_{s-1}}{2}$ and $h_0 = \mathcal{O}(1)$. This defines a hierarchy of nested spaces

$$\mathbf{H}_s^{k,r+1} := Y_\tau^k(I) \otimes \mathbf{V}_s^{r+1}(\Omega), \quad H_s^{k,r} := Y_\tau^k(I) \otimes Q_s^r(\Omega).$$

For brevity, we let $r \geq k$ as well as $k = 2^K$ and $r = 2^R$ for some $K, R \in \mathbb{N}$.

Grid transfer operators. By the mapping

$$(4.6) \quad P_{s-1 \rightarrow s}^h : \{\mathbf{V}_{s-1}^{r+1}(\Omega), Q_{s-1}^r(\Omega)\} \rightarrow \{\mathbf{V}_s^{r+1}(\Omega), Q_s^r(\Omega)\}$$

we denote the respective canonical embedding of the spacial finite element spaces into their refinement within the mesh hierarchy. For $\{\mathbf{v}_{\tau h}, p_{\tau h}\} \in Y_\tau^k(I_n) \otimes \mathbf{V}_{s-1}^{r+1}(\Omega) \times$

$Y_\tau^k(I_n) \otimes Q_s^r(\Omega)$, the matrix representation $\mathbf{P}_{s-1 \rightarrow s}^n \in \mathbb{R}^{(k+1) \cdot M_s, (k+1) \cdot M_{s-1}}$ of the geometric prolongation for space-time functions on I_n is the tensor product

$$\mathbf{P}_{s-1 \rightarrow s}^n := \mathbf{E}_{k+1} \otimes \mathbf{P}_{s-1 \rightarrow s}^h$$

for the vector representations of $\{\mathbf{v}_{\tau h}, p_{\tau h}\}$ on I_n , where $\mathbf{P}_{s-1 \rightarrow s}^h \in \mathbb{R}^{M_s, M_{s-1}}$ is the matrix representation of the prolongation (4.6) in space from \mathcal{T}_{s-1} to \mathcal{T}_s for $\mathbf{V}_{s-1}^{r+1}(\Omega)$ or $Q_{s-1}^r(\Omega)$, respectively, with M_s denoting the dimension of the finite element space.

Polynomial prolongation $P_{(k/2, r/2) \rightarrow (k, r)}^p = P_{k/2 \rightarrow k}^p \otimes P_{r/2 \rightarrow r}^p$ is defined by tensor products of the prolongations in the either variables. Its matrix representation is then defined by matrix products of tensor products of the form as in (4.6). Restrictions are chosen as the adjoint of the prolongation; cf. [21].

Cycle and coarsening order. We employ a V -cycle multigrid approach with ν_1/ν_2 pre-/post-smoothing steps due to its superior parallel scaling properties. Coarsening is done *firstly in the polynomial degree* (p), i.e. $(k, r) \mapsto (k/2, r/2)$ until $(1, 1)$ is reached, and *secondly geometrically for the space mesh* (h), i.e. $(s) \mapsto (s-1)$. We recall that h -multigrid for the temporal variable is not used here. If the p -hierarchy of the spatial variables is larger than of the temporal variable, then p -coarsening steps are done firstly until the hierarchy heights in space and time coincide; cf. [21] for the presentation of a pseudo algorithm. The coarsest problem is solved either directly or by FGMRES iterations. Corrections are prolonged in the reverse order.

This coarsening order follows the hp -STMG construction in [21] and preserves the tensor-product structure exploited by the patch-based smoother. Patch definitions and variants (element/vertex-star, treatment of pressure DoFs) are specified in Subsection 4.3 and in [21].

4.3. Inexact space-time Vanka smoother. The smoother is essential for the performance of multigrid methods. We use a local smoother of Vanka-type [32]. This smoother has proved its efficiency and scalability for saddle point problems [16, 34, 3, 21]. For its construction in the framework of space-time finite element methods we refer to [4, 5]. In particular, we use a local Vanka smoother that operates on the local slabs $S_n := K \times I_n$, for $K \in \mathcal{T}_s$. All global degrees of freedom linked to the element $K \in \mathcal{T}_d$ for all $(k+1)$ Gauss–Radau time points of I_n are updated simultaneously by the local Vanka systems. In our matrix-free approach, the global Jacobian matrix (3.24) is not explicitly built in the FGMRES iterations. Instead, a matrix-free evaluation is used; cf. Subsection 4.4. However, the Vanka smoother that works on the degrees of freedom of the local slabs S_n continues to be matrix-based. To accelerate its application (cf. [21]), an approximation of the Jacobian on S_n is used here. The construction of this inexact space-time Vanka smoother is presented now.

We consider a fixed level of the joint multigrid hierarchy of space-time polynomial order and spatial mesh refinement, introduced before. To simplify the notation, we omit the indices characterizing the respective subinterval I_n and multigrid level. On subinterval I_n , we consider solving a linear system of the form (cf. (4.1))

$$\mathcal{J}\mathbf{d} = \mathbf{r}$$

with the Jacobian matrix \mathcal{J} being defined in (3.24) and some residual or right-hand side vector \mathbf{r} . For this system, the local Vanka smoother is defined by

$$(4.7) \quad \mathcal{S}_{S_n}(\mathbf{d}) := \mathcal{R}_{S_n}\mathbf{d} + \omega \mathcal{J}_{S_n}^{-1} \mathcal{R}_{S_n}(\mathbf{r} - \mathcal{J}\mathbf{d}).$$

In (4.7), we denote by \mathcal{R}_{S_n} the local restriction operator that assigns to a global

defect vector \mathbf{d} the local block vector $\mathcal{R}_{S_n} \mathbf{d}$ that contains all components of \mathbf{d} that are associated with all degrees of freedom linked to the slab S_n . Further, the parameter $\omega > 0$ is an algorithmic relaxation parameter, and \mathcal{J}_{S_n} denotes the local Jacobian associated with the degrees of freedom on the slab S_n . The local Jacobian matrix \mathcal{J}_{S_n} inherits the block structure of its global counterpart in (3.24).

In (3.25a), the block diagonal matrix $\mathbf{H}'_n(\mathbf{V}_n)$, defined in (3.14), of the convective contribution depends on the block vectors \mathbf{V}_n^a of the velocity degrees of freedom at all time nodes $t_{n,a} \in I_n$, for $a = 1, \dots, k+1$. This feature is inherited by its local on K counterpart $\mathbf{H}'_{n,K}(\mathbf{V}_{n,K})$. It inflates both measures, setup cost and memory, of its evaluation. To reduce this, we consider using a surrogate $\widetilde{\mathbf{H}}'_{n,K}(\mathbf{V}_{n,K}^*)$, that evaluates the current solution in the midpoint t_n^* of I_n only. Thus, we substitute in the local Jacobian \mathcal{J}_{S_n} the contribution $\mathbf{H}'_{n,K}(\cdot)$ by

$$(4.8) \quad \widetilde{\mathbf{H}}'_{n,K}(\mathbf{V}_n^*) \coloneqq \text{diag}(\mathbf{H}'_K(\mathbf{V}_n^*), \dots, \mathbf{H}'_K(\mathbf{V}_n^*))$$

with $\mathbf{H}'_K(\cdot)$ denoting the local counterpart of $\mathbf{H}'(\cdot)$, defined in (3.13), and

$$(4.9) \quad \mathbf{V}_{n,K}^* = \sum_{a=1}^{k+1} \varphi_n^a(t_n^*) \sum_{i=1}^{M_K^v} V_{n,K,i}^a \chi_i^v \in \mathbf{V}_h^{r+1},$$

where M_K^v denotes the number of local velocity degrees of freedom on K . On each slab S_n , the spatial core $\mathbf{H}'_K(\mathbf{V}_n^*)$ is thus *shared* across all time nodes. For the set of velocity and pressure degrees of freedom of size $m \simeq d(r+2)^d + (r+1)^d$, factorization and storage is thus needed only once per slab with computational cost $\mathcal{O}(m^3)$ and memory usage $\mathcal{O}(m^2)$, instead of $(k+1)$ times. This is essential for memory-friendly and cache-efficient implementations. Letting $\widetilde{\mathcal{J}}_{S_n}$ denote the resulting surrogate of \mathcal{J}_{S_n} in (4.7), assembled by using (4.8), a single local Vanka sweep reads as

$$(4.10) \quad \mathbf{d} \leftarrow \mathbf{d} + \omega \sum_K \mathbf{R}_{S_n}^\top (\widetilde{\mathcal{J}}_{S_n})^{-1} \mathbf{R}_{S_n} (\mathbf{r} - \mathcal{J} \mathbf{d}),$$

where \mathbf{R}_{S_n} is the matrix representation of \mathcal{R}_{S_n} in (4.7).

Remark 4.1. The Jacobian of the nonlinear term $\mathbf{N}_{\Gamma_D}^{\mathbf{v},c}(\mathbf{V}_n)$ in (3.22a), that is due to the boundary pairings with the convective term in (2.11), is approximated similarly by a surrogate.

Finally, we analyze the surrogate (4.8). We aim to characterize the perturbation of the performance of the local Vanka smoother by building the Jacobian on the approximation (4.8) to (3.14). In order not to overload this work, we use some simplifying assumptions about $\mathbf{H}'(\cdot)$ and \mathbf{V}_n^* , without proving them explicitly. Their rigorous proof is left as a work for the future. The contribution $\mathbf{N}_{\Gamma_D}^{\mathbf{v},c}(\mathbf{V}_n)$ is also neglected. Nevertheless, Lemma 4.2 illustrates advantageous properties of the surrogate based on (4.8) and, thereby, suggests its application. In the following, all matrix norms are spectral (operator) norms. For a given matrix \mathbf{A} , let $s_{\min}(\mathbf{A})$ and $s_{\max}(\mathbf{A})$ denote its smallest and largest singular values, respectively, i.e., $s_{\max}(\mathbf{A}) = \|\mathbf{A}\|$ and, if \mathbf{A} is invertible, $s_{\min}(\mathbf{A}) = \|\mathbf{A}^{-1}\|^{-1}$.

LEMMA 4.2 (Characterization of local Vanka surrogate). *Consider a slab S_n with spatial element K . Let $\mathbf{S}_n \coloneqq \mathcal{J}_{S_n} \in \mathbb{R}^{(k+1) \cdot (M_K^v + M_K^p), (k+1) \cdot (M_K^v + M_K^p)}$, with $M_K^v + M_K^p$ denoting the total number of velocity and pressure degrees of freedom on K , be the exact local Vanka matrix of (4.7) on $K \in \mathcal{T}_h$. Let $\widetilde{\mathbf{S}}_n \in \mathbb{R}^{(k+1) \cdot (M_K^v + M_K^p), (k+1) \cdot (M_K^v + M_K^p)}$*

be its surrogate based on the convective contribution (4.8). Assume local Lipschitz continuity of the local Jacobian matrix $\mathbf{H}'_K(\cdot) \in \mathbb{R}^{M_K^v, M_K^v}$ on K , such that

$$(4.11) \quad \|\mathbf{H}'_K(\mathbf{U}_K) - \mathbf{H}'_K(\mathbf{V}_K)\| \leq L_K \|\mathbf{U}_K - \mathbf{V}_K\| \quad \text{for } \mathbf{U}_K, \mathbf{V}_K \in \mathbb{R}^{M_K^v}.$$

Let $a \in \{1, \dots, k+1\}$. For $\mathbf{V}_{n|K}(t_n^a)$, $\mathbf{V}_{n|K}(t_n^*) \in \mathbb{R}^{r+1}(K)$, represented by $\mathbf{V}_{n,K}^a \in \mathbb{R}^{M_K^v}$ and $\mathbf{V}_{n,K}^* \in \mathbb{R}^{M_K^v}$, respectively, assume the approximation property that

$$(4.12) \quad \|\mathbf{V}_{n,K}^a - \mathbf{V}_{n,K}^*\| \leq C_K \tau_n.$$

Then the local perturbation $\mathbf{E}_n := \tilde{\mathbf{S}}_n - \mathbf{S}_n$ satisfies that

$$(4.13) \quad \|\mathbf{E}_n\| \leq C \tau_n, \quad C := c C_K L_K \|\mathbf{M}_n^\tau\|,$$

where c is independent of the step sizes k and τ_n . Let

$$(4.14) \quad \|\mathbf{E}_n\| \leq \varepsilon_n \|\mathbf{S}_n^{-1}\|^{-1}, \text{ with some } \varepsilon_n < 1.$$

Then there holds the following.

(i) **Nonsingularity and inverse bound.** The matrix $\tilde{\mathbf{S}}_n$ is invertible and

$$\|\tilde{\mathbf{S}}_n^{-1}\| \leq (1 - \varepsilon_n)^{-1} \|\mathbf{S}_n^{-1}\|.$$

(ii) **Approximation property.** There holds that

$$\|\mathbf{I} - \mathbf{S}_n^{-1} \tilde{\mathbf{S}}_n\| \leq \varepsilon_n.$$

Hence the spectrum and the field of values satisfy that

$$\sigma(\mathbf{S}_n^{-1} \tilde{\mathbf{S}}_n) \subset \{z \in \mathbb{C} : |z - 1| \leq \varepsilon_n\}, \quad \mathcal{W}(\mathbf{S}_n^{-1} \tilde{\mathbf{S}}_n) \subset \{z \in \mathbb{C} : |z - 1| \leq \varepsilon_n\}.$$

(iii) **Singular-value (conditioning) bounds.** For the minimal and maximal singular values there holds that

$$(1 - \varepsilon_n) s_{\min}(\mathbf{S}_n) \leq s_{\min}(\tilde{\mathbf{S}}_n) \leq s_{\max}(\tilde{\mathbf{S}}_n) \leq (1 + \varepsilon_n) s_{\max}(\mathbf{S}_n).$$

Proof. The Lipschitz continuity (4.11) along with the local on K approximation property (4.12) directly proves the assertion (4.13). The Neumann series expansion of matrices directly proves item (i) and the approximation property in item (ii). Since every eigenvalue λ of $\mathbf{S}_n^{-1} \tilde{\mathbf{S}}_n$ satisfies that $|\lambda| \leq \|\mathbf{S}_n^{-1} \tilde{\mathbf{S}}_n\|$, the spectrum of $\mathbf{I} - \mathbf{S}_n^{-1} \tilde{\mathbf{S}}_n$ lies in the ball of radius ε_n around 1, and the field-of-values inclusion follows directly. To show item (iii), we use that $s_{\min}(\mathbf{AB}) \geq s_{\min}(\mathbf{A}) s_{\min}(\mathbf{B})$ and $s_{\max}(\mathbf{AB}) \leq s_{\max}(\mathbf{A}) s_{\max}(\mathbf{B})$. Further we have the product representation $\tilde{\mathbf{S}}_n = \mathbf{S}_n(\mathbf{I} + \mathbf{S}_n^{-1} \mathbf{E}_n)$. By means of (4.14), we then get that

$$s_{\max}(\tilde{\mathbf{S}}_n) \leq (1 + \varepsilon_n) s_{\max}(\mathbf{S}_n).$$

The lower bound for $s_{\min}(\tilde{\mathbf{S}}_n)$ follows similarly. \square

Remark 4.3 (On the results of Lemma 4.2).

- If $\varepsilon_n = \mathcal{O}(\tau_n)$ by means of (4.13), we conclude that the midpoint surrogate $\tilde{\mathbf{S}}_n$ and the exact local Jacobian \mathbf{S}_n are uniformly close to each other (in operator norm, spectrum, field of values, and singular values).

- The condition (4.12) controls on slab $S_n = K \times I_n$ the distance between $\mathbf{V}_{n|K}(t_n^a) \in \mathbf{V}^{r+1}(K)$ and $\mathbf{V}_{n|K}(t_n^*) \in \mathbf{V}^{r+1}(K)$ in the Euclidian norm of their coefficient vectors. Norm equivalence between the $L^2(K)$ norm of finite element functions and the vector norm of their coefficients in the finite element basis is enured, but h_K dependent,

$$c_1 h_K^{d/2} \|\mathbf{V}\| \leq \|\mathbf{v}_h\|_{L^2(K)} \leq c_2 h_K^{d/2} \|\mathbf{V}\|,$$

for $\mathbf{v}_h = \sum_{j=1}^{M_K} V_j \boldsymbol{\chi}_{K,j}^v \in \mathbf{V}^{r+1}(K)$ and $\mathbf{V} = (V_1, \dots, V_{M_K})^\top$. For brevity, we do not incorporate this into Assumption (4.12), since a rigorous $L^2(\Omega)$ error estimate and the induced bound on the distance of coefficient vectors is beyond the scope of this work. We defer such an analysis to future work.

- In Lemma 4.2, (i) guarantees that for the patch matrix the evaluation of the convective part in the midpoint does not deteriorate the local patch solve and controls its inverse, (ii) shows that the frozen patch acts as a near-identity preconditioner for the exact patch (so the Vanka update remains effective), and (iii) quantifies that conditioning, and thus damping properties, deviate by at most $\mathcal{O}(\tau_n)$, which is then kept small in practice by our rebuild triggers. Precisely, the smoother is *rebuilt* using an updated \mathbf{U}_n^* to reduce ε_n when convergence deteriorates. Let

$$\rho_m := \frac{\|\mathcal{R}_n(\mathbf{U}_n^m; \mathbf{V}_{n-1})\|_{\mathcal{M}}}{\|\mathcal{R}_n(\mathbf{U}_n^{m-1}; \mathbf{V}_{n-1})\|_{\mathcal{M}}},$$

and κ_m the number of FGMRES iterations required until the inexactness test (4.2) is first met. Then, choose thresholds $\theta_N > 1$, $\theta_L > 1$, an absolute cap κ_{abs} , and a stagnation window (s, ϑ) . We rebuild if $\rho_m \geq \theta_N \rho_{m-1}$ (Newton deterioration), or $\kappa_m \geq \max(\theta_L \kappa_{m-1}, \kappa_{\text{abs}})$ (linear deterioration), or if FGMRES residuals stagnate with $\|r_{j+1}\|/\|r_j\| \geq \vartheta$ for s consecutive inner iterations.

4.4. Matrix-free operator evaluation. In this work, linear operators are evaluated without the explicit formation and storage of system matrices. For this, we rely on the matrix-free multigrid framework in the **deal.II** library [2, 19, 24, 9]. All matrix-vector products $\mathbf{Y} = \mathbf{S} \mathbf{X}$ for solving Problem 3.4 are computed via global accumulation of element-wise operations,

$$\mathbf{S} \mathbf{X} = \sum_{c=1}^{n_c} \mathbf{R}_{c, \text{loc-glob}}^\top \mathbf{S}_c \mathbf{R}_{c, \text{loc-glob}} \mathbf{X}, \quad \mathbf{S}_c = \mathbf{B}_c^\top \mathbf{D}_c \mathbf{B}_c,$$

where $\mathbf{R}_{c, \text{loc-glob}}$ maps local degrees of freedom to global indices, \mathbf{B}_c contains shape function and gradient evaluations, and \mathbf{D}_c encodes quadrature weights and material/ flux coefficients. Sum-factorization reduces multi-dimensional kernels to products of one-dimensional operations; vectorization further accelerates the evaluation. These techniques are used for the spatial operators in Problem 3.4 and their Jacobians (3.24)–(3.25). The temporal matrices in (3.22) are precomputed as in [22, 21]. Products such as $(\mathbf{M}^\top \otimes \mathbf{A}_h) \mathbf{V}$ are evaluated by computing $\mathbf{A}_h \mathbf{V}^a$ once per temporal DoF a , followed by small block multiplications with the temporal matrices; this extends to all Kronecker products in (3.22).

Navier–Stokes: matrix-free application of the slab Jacobian. For Navier–Stokes, we apply the (state-dependent) slab Jacobian $\mathcal{J}_n(\mathbf{U}_n)$ from (3.24)–(3.25) in a matrix-free fashion. We fully reuse the slab block notation (3.5). The only state dependence enters through the velocity-velocity block $\mathcal{J}_n^{1,1}(\mathbf{U}_n)$, and, by (3.14), this dependence

is *block diagonal in time*. Consequently, all state-dependent spatial kernels are evaluated independently for each temporal basis index and are then combined by dense multiplications with the temporal matrices $\mathbf{K}_n^\tau, \mathbf{M}_n^\tau$ from (A.1).

Concretely, given an increment $(\mathbf{V}_n, \mathbf{P}_n)$ with subvectors $\mathbf{V}_n^a \in \mathbb{R}^{M^v}, \mathbf{P}_n^a \in \mathbb{R}^{M^p}$ ($a = 1, \dots, k+1$), the product $(\mathbf{Y}_{n,v}, \mathbf{Y}_{n,p}) = \mathcal{J}_n(\mathbf{U}_n)(\mathbf{V}_n, \mathbf{P}_n)$ is computed as follows:

1. *Column-wise spatial products (matrix-free)*. For each $a = 1, \dots, k+1$, compute the spatial actions that appear in (3.25a)–(3.25b),

$$\mathbf{q}^{(a)} := \mathbf{M}_h \mathbf{V}_n^a, \quad \mathbf{d}^{(a)} := \mathbf{B} \mathbf{V}_n^a, \quad \mathbf{g}^{(a)} := \mathbf{B}^\top \mathbf{P}_n^a,$$

and evaluate the state-dependent velocity contribution of $\mathcal{J}_n^{1,1}(\mathbf{U}_n)$ at the same temporal block, i.e.,

$$\mathbf{w}^{(a)} := \left[\mathcal{J}_n^{1,1}(\mathbf{U}_n) \right]^{a,a} \mathbf{V}_n^a,$$

where this “diagonal block” comprises the viscous part, linearized convection, and boundary terms (e.g. Nitsche/outflow), with coefficients evaluated on-the-fly from the current Newton state \mathbf{U}_n .

2. *Dense temporal mixing*. Accumulate for each row index $i = 1, \dots, k+1$:

$$\mathbf{Y}_{n,v}^i += \sum_{a=1}^{k+1} (\mathbf{K}_n^\tau)_{ia} \mathbf{q}^{(a)} + \sum_{a=1}^{k+1} (\mathbf{M}_n^\tau)_{ia} (\mathbf{w}^{(a)} + \mathbf{g}^{(a)}), \quad \mathbf{Y}_{n,p}^i += \sum_{a=1}^{k+1} (\mathbf{M}_n^\tau)_{ia} \mathbf{d}^{(a)}.$$

The coupling induced by the jump matrix \mathbf{C}_n^τ (see (A.1b)) is implemented as a separate, purely temporal update with \mathbf{M}_h . The midpoint surrogate is *only* used inside the Vanka smoother to enable reuse of patch factorizations and does not modify the outer Jacobian application.

5. Numerical experiments. We assess the proposed monolithic Navier-Stokes Newton-Krylov solver in the fully discrete setting of Section 2, using spatial $\mathbb{Q}_{r+1}/\mathbb{P}_r^{\text{disc}}$ pairs and a DG(k) discretization in time. The nonlinear systems are solved by the inexact Newton-Krylov method of Section 4 (Eisenstat-Walker forcing, Armijo backtracking), where FGMRES is preconditioned by a single V -cycle of the hp space-time multigrid (STMG) with Vanka smoothing (Subsection 4.2).

Our primary goal is robustness of both the *outer* Newton iterations and the *inner* linear iterations with respect to mesh size h , polynomial degree p , and moderate Reynolds numbers. We assess robustness by (i) the total number of Newton steps and (ii) the average number of FGMRES iterations per Newton step. Specifically, we call the method **h/p -robust in Newton** if the number of Newton steps required to meet (4.2) remains essentially bounded as $h \downarrow 0$ and $p \uparrow$, and **h/p -robust in FGMRES** if the FGMRES iteration count *per Newton step* remains essentially bounded under the same refinement. We call it **Re-robust** if, over the target range $\text{Re} \in [1, 10^4]$, both Newton and FGMRES iteration counts remain controlled. We report the average number of Newton steps \bar{n}_{NL} and the average FGMRES iterations per Newton step \bar{n}_{L} versus ν . Such robustness is crucial for linear complexity in the number of global degrees of freedom and mitigates memory pressure from the Arnoldi basis in FGMRES. In our experiments, the method remains within memory limits.

All tests were executed on the HSUper cluster (Helmut Schmidt University) with 571 nodes, each with two Intel Xeon Platinum 8360Y CPUs (36 cores per CPU) and 256 GB RAM. In our experiments the number of MPI processes always match the physical cores. The source code is available [20]. Unless stated otherwise, we use the

following setting for the Newton. The relative and absolute residual tolerances for Newton are 10^{-8} and 10^{-12} . The parameters for the Armijo line search are an initial step of $\lambda_0 = 1$, an Armijo constant $c = 10^{-4}$, a backtracking factor $\tau = 0.5$, at most 5 backtracks, and a minimum step $\alpha_{\min} = 10^{-3}$. We employ the nonmonotone variant with window size $M = 5$. For the *Eisenstat-Walker forcing* we choose the initial η as $\eta_0 = 0.4$ $\eta \in [\eta_{\min}, \eta_{\max}]$ with $\eta_{\min} = 10^{-3}$ and $\eta_{\max} = 0.8$, and set $c_{\eta} = 0.5$ and $\theta = 1.5$. The FGMRES solver is steered completely by the Eisenstat-Walker forcing. However, we impose a limit of 50 iterations which we do not hit in any of our experiments. The penalty parameters for Nitsche's method must be sufficiently large for correct enforcement of the boundary conditions. Here, we choose $\gamma_1 = \gamma_2 = 10$.

Table 1: Errors for $\mathbb{Q}_{r+1}^2/\mathbb{P}_r^{\text{disc}}/\text{DG}(r)$ discretizations of the Navier-Stokes system for (5.1a) with $\nu = 10^{-2}$

(a) Calculated velocity and pressure errors in the space-time L^2 -norm with eoc.

h	$r = 3$				$r = 4$			
	$e_{L^2(L^2)}^v$	eoc	$e_{L^2(L^2)}^p$	eoc	$e_{L^2(L^2)}^v$	eoc	$e_{L^2(L^2)}^p$	eoc
2^{-1}	$2.800 \cdot 10^{-2}$	-	$1.341 \cdot 10^{-2}$	-	$1.729 \cdot 10^{-3}$	-	$1.049 \cdot 10^{-3}$	-
2^{-2}	$1.274 \cdot 10^{-3}$	4.46	$7.377 \cdot 10^{-4}$	4.18	$1.761 \cdot 10^{-4}$	3.30	$1.151 \cdot 10^{-4}$	3.19
2^{-3}	$4.930 \cdot 10^{-5}$	4.69	$4.784 \cdot 10^{-5}$	3.95	$3.266 \cdot 10^{-6}$	5.75	$3.638 \cdot 10^{-6}$	4.98
2^{-4}	$1.621 \cdot 10^{-6}$	4.93	$2.988 \cdot 10^{-6}$	4.00	$5.388 \cdot 10^{-8}$	5.92	$1.134 \cdot 10^{-7}$	5.00
2^{-5}	$5.128 \cdot 10^{-8}$	4.98	$1.863 \cdot 10^{-7}$	4.00	$8.549 \cdot 10^{-10}$	5.98	$3.527 \cdot 10^{-9}$	5.01

(b) Calculated velocity errors in the space-time $L^2(H^1)$ -norm and divergence with eoc.

h	$r = 3$				$r = 4$			
	$e_{L^2(H^1)}^v$	eoc	$e_{L^2(L^2)}^{\nabla \cdot v}$	eoc	$e_{L^2(H^1)}^v$	eoc	$e_{L^2(L^2)}^{\nabla \cdot v}$	eoc
2^{-1}	$6.945 \cdot 10^{-1}$	-	$5.805 \cdot 10^{-1}$	-	$5.231 \cdot 10^{-2}$	-	$4.705 \cdot 10^{-2}$	-
2^{-2}	$5.483 \cdot 10^{-2}$	3.66	$4.963 \cdot 10^{-2}$	3.55	$8.948 \cdot 10^{-3}$	2.55	$8.311 \cdot 10^{-3}$	2.50
2^{-3}	$4.003 \cdot 10^{-3}$	3.78	$3.815 \cdot 10^{-3}$	3.70	$3.249 \cdot 10^{-4}$	4.78	$3.141 \cdot 10^{-4}$	4.73
2^{-4}	$2.540 \cdot 10^{-4}$	3.98	$2.474 \cdot 10^{-4}$	3.95	$1.071 \cdot 10^{-5}$	4.92	$1.048 \cdot 10^{-5}$	4.90
2^{-5}	$1.588 \cdot 10^{-5}$	4.00	$1.557 \cdot 10^{-5}$	3.99	$3.400 \cdot 10^{-7}$	4.98	$3.344 \cdot 10^{-7}$	4.97

5.1. Convergence test. As a first test case, we consider a model problem on the space-time domain $\Omega \times I = [0, 1]^2 \times [0, 1]$ with prescribed solution given for the velocity $\mathbf{v}: \Omega \times I \rightarrow \mathbb{R}^2$ and pressure $p: \Omega \times I \rightarrow \mathbb{R}$ by

$$(5.1a) \quad \mathbf{v}(\mathbf{x}, t) = \sin(t) \begin{pmatrix} \sin^2(\pi x) \sin(\pi y) \cos(\pi y) \\ \sin(\pi x) \cos(\pi x) \sin^2(\pi y) \end{pmatrix},$$

$$(5.1b) \quad p(\mathbf{x}, t) = \sin(t) \sin(\pi x) \cos(\pi x) \sin(\pi y) \cos(\pi y).$$

We choose the kinematic viscosity as $\nu \in \{10^{-2}, 10^{-4}, 10^{-6}\}$ and choose the external force \mathbf{f} such that the solution (5.1) satisfies (2.1). The initial velocity is prescribed as zero and homogeneous Dirichlet boundary conditions are imposed on $\partial\Omega$ for all times

$$\mathbf{v} = \mathbf{0} \text{ on } \Omega \times \{0\}, \quad \mathbf{v} = \mathbf{0}, \text{ on } \partial\Omega \times (0, T].$$

The space-time mesh $\mathcal{T}_h \otimes \mathcal{M}_\tau$ is a uniform triangulation of the space-time domain $\Omega \times I$. We use discretizations with varying polynomial degrees $r \in \{1, 3, \dots, 6\}$ in space and $k = r$ in time to test the convergence.

Table 2: Average number of Newton iterations \bar{n}_{NL} per timestep (left) and average number of FGMRES iterations per Newton step \bar{n}_L (right) until convergence for polynomial degrees r and number of refinements c with $\mathbb{Q}_{r+1}^2/\mathbb{P}_r^{\text{disc}}/\text{DG}(r)$ discretization.

(a) Results for $\nu = 10^{-2}$, i.e. $\text{Re} = 100$.

$r \setminus c$	1	2	3	4	5	6	$r \setminus c$	1	2	3	4	5	6
1	6.00	5.25	4.75	4.00	4.00	3.34	1	5.71	4.79	3.83	3.75	3.00	2.60
2	6.00	5.00	4.00	3.09	3.00	3.00	2	5.96	4.55	3.86	3.05	2.91	2.58
3	7.00	5.00	4.18	4.00	4.00	4.00	3	7.43	6.85	4.96	4.31	3.23	4.61
4	6.75	5.00	4.00	4.00	4.00	4.00	4	8.04	6.35	4.50	3.25	2.50	2.00
5	6.75	5.00	4.00	3.72	3.00	3.00	5	10.56	7.30	6.14	4.19	4.00	3.19
6	6.75	4.75	3.81	3.00	4.00	4.00	6	11.11	8.21	5.16	4.64	3.00	2.74

(b) Results for $\nu = 10^{-4}$, i.e. $\text{Re} = 1 \cdot 10^3$.

$r \setminus c$	1	2	3	4	5	6	$r \setminus c$	1	2	3	4	5	6
1	5.75	5.88	5.00	4.00	4.00	4.00	1	6.65	5.17	4.51	4.00	3.27	2.62
2	6.50	5.88	4.38	4.00	3.00	3.00	2	5.96	4.85	4.23	4.22	3.66	2.86
3	7.25	5.75	4.00	4.00	4.00	3.93	3	8.48	6.59	6.89	5.41	4.16	2.76
4	7.00	5.75	4.68	3.97	3.34	3.30	4	7.75	6.22	5.07	4.76	4.01	3.04
5	7.75	5.75	4.88	4.00	3.95	3.25	5	9.97	7.09	6.21	5.95	4.60	3.79
6	7.75	5.75	4.00	3.94	3.00	3.00	6	10.03	7.09	6.31	5.33	5.04	4.00

(c) Results for $\nu = 10^{-4}$, i.e. $\text{Re} = 1 \cdot 10^4$.

$r \setminus c$	1	2	3	4	5	6	$r \setminus c$	1	2	3	4	5	6
1	6.50	6.38	5.00	4.00	4.00	4.00	1	6.35	4.93	4.78	4.11	3.39	2.79
2	7.38	6.88	5.00	4.00	3.00	3.00	2	5.75	4.43	4.19	4.52	4.85	4.28
3	7.75	7.00	4.00	4.00	3.09	3.00	3	7.30	6.95	6.63	5.88	5.35	4.75
4	8.25	7.13	5.00	4.00	3.97	3.63	4	6.80	6.25	5.30	5.04	4.15	3.50
5	8.50	7.50	4.94	4.00	3.83	3.42	5	8.35	7.00	6.61	6.14	5.25	4.44
6	8.50	7.50	4.81	4.00	3.69	3.59	6	9.75	7.33	6.30	5.59	5.06	4.22

Table 1 shows the findings of our convergence study for $r \in \{3, 4\}$. The expected orders of convergence agree with the experimental rates. A complete set of results is provided in Figure C.1 in Appendix C. The $L^2(0, T; L^2(\Omega)^d)$ velocity error does not always attain the ideal rate $r+2$ due to the temporal polynomial degree k , whereas the $L^2(0, T; H^1(\Omega)^d)$ norm consistently exhibits the optimal order $r+1$, which supports the choice $k=r$ in time for the tests below.

Table 2 reports the nonlinear and linear iteration counts for these experiments: the number of Newton steps, and the average FGMRES iterations per Newton step when preconditioned by a single V -cycle hp STMG. The method shows excellent h - and p -robustness of both the Newton method and the inner Krylov solver. As the viscosity decreases (moderately increasing the Reynolds number), we observe no significant growth in outer Newton iterations and inner FGMRES iterations, indicating good Re -robustness of the solver in the studied range. The Armijo globalization and Eisenstat-Walker forcing are effective. We note that the rebuild of the Vanka-smoother was always triggered by slow Newton convergence, and the linear solver was not affected by the inexact smoother.

While polynomial coarsening ($r \rightarrow r-1$) can reduce FGMRES iterations, wall-clock gains may be limited by slowly shrinking local block sizes; we therefore use degree halving ($r \rightarrow r/2$), as also advocated in our previous work [21]. We use a single

smoothing step on all levels, i.e., $\nu_1 = \nu_2 = 1$. Additional smoothing can reduce the number of FGMRES iterations and may decrease the need for smoother rebuilds. In our computations, however, we typically rebuild the smoother only once per time step, so larger ν_1, ν_2 would increase the cost of each smoother application; see (4.7). Keeping the number of smoothing steps small is therefore critical for overall performance (cf. [22]). In the present section, we achieve excellent h -, p -, and Re-robustness. We revisit this trade-off in the next section on large-scale simulations and assess whether increased smoothing improves robustness in practice.

Table 3: Discretization sizes for refinement levels c and polynomial degrees r : number of global space-time elements (# st-elements) and total number of unknowns N_{dof} .

c	# st-elements	N_{dof}		
		$r = 2$	$r = 3$	$r = 4$
4	$1.049 \cdot 10^6$	$3.025 \cdot 10^8$	$9.275 \cdot 10^8$	$2.252 \cdot 10^9$
5	$1.678 \cdot 10^7$	$4.709 \cdot 10^9$	$1.453 \cdot 10^{10}$	$3.604 \cdot 10^{10}$
6	$2.684 \cdot 10^8$	$7.431 \cdot 10^{10}$	$2.362 \cdot 10^{11}$	$5.766 \cdot 10^{11}$
7	$4.295 \cdot 10^9$	$1.181 \cdot 10^{12}$	$3.779 \cdot 10^{12}$	$9.225 \cdot 10^{12}$

Table 4: Iteration counts for the nonlinear solve for different numbers of smoothing steps n_{sm} and kinematic viscosities ν : average number of Newton iterations \bar{n}_{NL} and average number of FGMRES iterations per Newton step \bar{n}_{L} for polynomial degrees r and refinements c . Problem sizes (# st-elements, N_{dof}) are given in Table 3.

(a) Linear and nonlinear iteration counts for $\nu = 4 \cdot 10^{-4}$ and $n_{\text{sm}} = \nu_1 = \nu_2 \in \{1, 2\}$ (left/right)

c	$r = 2$		$r = 3$		$r = 4$	
	\bar{n}_{NL}	\bar{n}_{L}	\bar{n}_{NL}	\bar{n}_{L}	\bar{n}_{NL}	\bar{n}_{L}
4	5.00	2.61	5.00	3.42	5.11	3.55
5	5.00	2.15	5.00	2.83	4.99	2.95
6	4.99	1.91	4.96	2.17	4.99	2.88
7	4.98	1.90	4.93	2.11	4.96	2.58

c	$r = 2$		$r = 3$		$r = 4$	
	\bar{n}_{NL}	\bar{n}_{L}	\bar{n}_{NL}	\bar{n}_{L}	\bar{n}_{NL}	\bar{n}_{L}
4	5.00	1.66	5.00	2.08	4.99	2.51
5	5.00	1.52	4.99	1.71	4.94	1.76
6	4.96	1.38	4.95	1.57	4.89	1.72
7	4.90	1.26	4.88	1.47	4.81	1.70

(b) Linear and nonlinear iteration counts for $\nu = 2 \cdot 10^{-4}$ and $n_{\text{sm}} = \nu_1 = \nu_2 \in \{1, 2\}$ (left/right)

c	$r = 2$		$r = 3$		$r = 4$	
	\bar{n}_{NL}	\bar{n}_{L}	\bar{n}_{NL}	\bar{n}_{L}	\bar{n}_{NL}	\bar{n}_{L}
4	4.99	2.65	4.99	3.47	5.09	3.60
5	4.99	2.18	4.99	2.87	4.99	2.99
6	4.98	1.94	4.96	2.20	4.99	2.92
7	4.98	1.93	4.93	2.14	4.96	2.62

c	$r = 2$		$r = 3$		$r = 4$	
	\bar{n}_{NL}	\bar{n}_{L}	\bar{n}_{NL}	\bar{n}_{L}	\bar{n}_{NL}	\bar{n}_{L}
4	4.99	1.67	4.99	2.10	4.99	2.59
5	4.99	1.53	4.99	1.69	4.93	1.77
6	4.97	1.35	4.95	1.51	4.89	1.70
7	4.89	1.25	4.86	1.42	4.77	1.63

5.2. Lid-driven cavity flow. We now study the benchmark problem of lid-driven cavity flow. The space-time mesh $\mathcal{T}_h \times \mathcal{M}_\tau$ is a uniform triangulation of the space-time domain $\Omega \times I = [0, 1]^3 \times [0, 8]$, refined globally c times. A Dirichlet profile \mathbf{v}_D is prescribed at the upper boundary $\Gamma_D = [0, 1]^2 \times \{1\} \subset \partial\Omega$ by

$$\mathbf{v}_D(x, y, z, t) = \sin\left(\frac{\pi}{4}t\right) \quad \text{on } \Gamma_D \times [0, 8],$$

Table 5: Throughput θ and wall time for different values of ν , n_{sm} , r and c . Problem sizes (# st-elements, N_{dof}) are reported in Table 3.

(a) Throughput for $\nu = 4 \cdot 10^{-4}$ and $n_{\text{sm}} = \nu_1 = \nu_2 \in \{1, 2\}$ (left/right)

c	$r = 2$	$r = 3$	$r = 4$	c	$r = 2$	$r = 3$	$r = 4$
4	$1.200 \cdot 10^6$	$9.867 \cdot 10^5$	$8.001 \cdot 10^5$	4	$1.080 \cdot 10^6$	$9.005 \cdot 10^5$	$6.624 \cdot 10^5$
5	$3.294 \cdot 10^6$	$2.750 \cdot 10^6$	$2.050 \cdot 10^6$	5	$3.093 \cdot 10^6$	$2.892 \cdot 10^6$	$1.716 \cdot 10^6$
6	$1.142 \cdot 10^7$	$7.910 \cdot 10^6$	$6.200 \cdot 10^6$	6	$1.013 \cdot 10^7$	$6.320 \cdot 10^6$	$5.148 \cdot 10^6$
7	$3.578 \cdot 10^7$	$2.553 \cdot 10^7$	$1.800 \cdot 10^7$	7	$2.811 \cdot 10^7$	$1.889 \cdot 10^7$	$1.419 \cdot 10^7$

(b) Throughput for $\nu = 2 \cdot 10^{-4}$ and $n_{\text{sm}} = \nu_1 = \nu_2 \in \{1, 2\}$ (left/right)

c	$r = 2$	$r = 3$	$r = 4$	c	$r = 2$	$r = 3$	$r = 4$
4	$1.311 \cdot 10^6$	$1.078 \cdot 10^6$	$8.738 \cdot 10^5$	4	$1.209 \cdot 10^6$	$1.008 \cdot 10^6$	$7.412 \cdot 10^5$
5	$3.597 \cdot 10^6$	$3.004 \cdot 10^6$	$2.239 \cdot 10^6$	5	$3.461 \cdot 10^6$	$3.236 \cdot 10^6$	$1.920 \cdot 10^6$
6	$1.256 \cdot 10^7$	$8.698 \cdot 10^6$	$6.817 \cdot 10^6$	6	$1.268 \cdot 10^7$	$7.915 \cdot 10^6$	$6.446 \cdot 10^6$
7	$3.934 \cdot 10^7$	$2.807 \cdot 10^7$	$1.979 \cdot 10^7$	7	$3.520 \cdot 10^7$	$2.366 \cdot 10^7$	$1.777 \cdot 10^7$

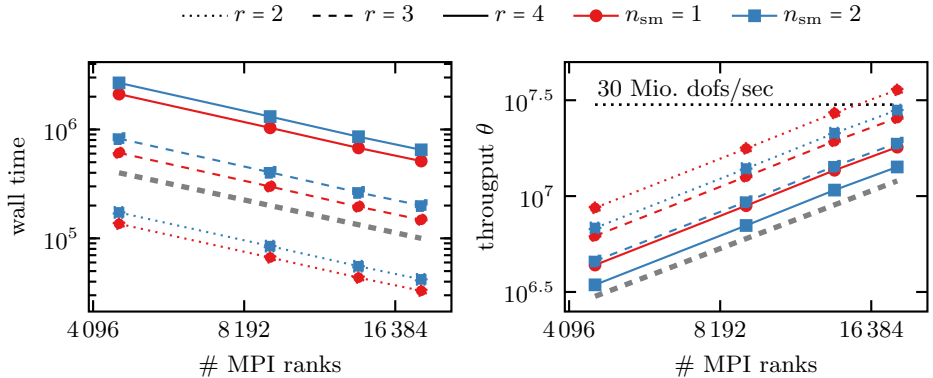


Fig. 1: Strong scaling test results for the STMG algorithm with varying numbers of smoothing steps (anchored to the $c = 7$ case at 18432 MPI ranks, cf. Table 5). The left plot shows the time to solution over the number of MPI processes. The dashed gray lines indicate the optimal scaling. The right plot depicts the degrees of freedom (dofs) processed per second over the number of MPI processes.

and no-slip conditions are imposed on $\Gamma_{\text{wall}} = \partial\Omega \setminus \Gamma_D$. We consider $\nu \in \{2 \cdot 10^{-4}, 4 \cdot 10^{-4}\}$ and degree $r \in \{2, 3, 4\}$ in space with $k = r$ in time. For the strong scaling test in Figure 1 we fix $c = 7$, i.e. $2.097 \cdot 10^6$ space elements and 2048 time elements; cf. Table 3.

Iterations and robustness. The nonlinear solve is stable across all configurations: the average Newton counts remain essentially constant (about five iterations) for both viscosities and all degrees, see Table 4. The average FGMRES iterations per Newton step are likewise well controlled and decrease mildly with refinement, indicating mesh-independent preconditioning. Increasing the smoothing steps from $n_{\text{sm}} = 1$ to $n_{\text{sm}} = 2$ consistently reduces linear iterations for both viscosities and all degrees (most noticeably for larger r), i.e. additional smoothing improves p -robustness, although

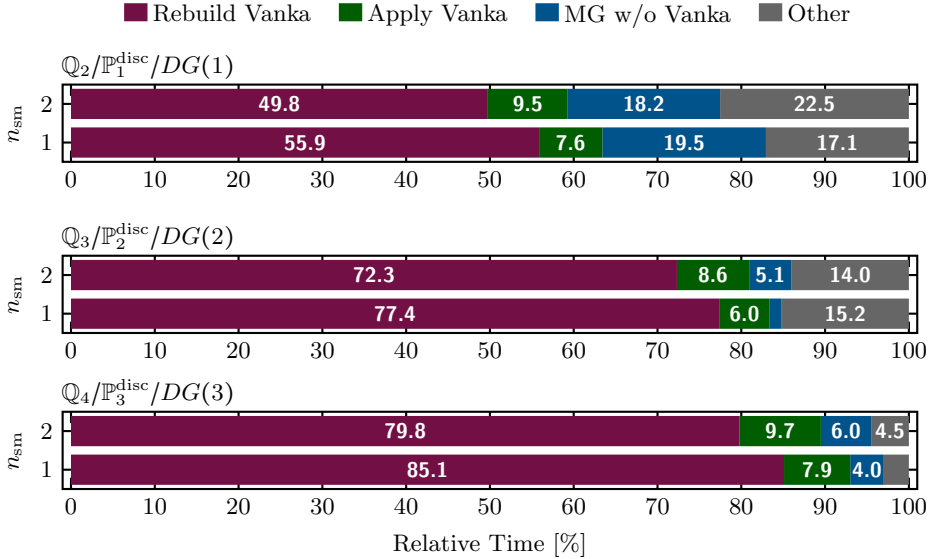


Fig. 2: Relative time spent in dominant parts of the Navier-Stokes solve on 18432 MPI ranks. The cell-wise Vanka smoother is dominated by the expensive rebuild and application of the Vanka smoother. Data shown for $c = 7$, $r \in \{2, 3, 4\}$, $n_{\text{sm}} \in \{1, 2\}$.

some degree dependence remains visible in Table 4.

Time to solution and throughput. We quantify performance by the throughput $\theta(n_{\text{sm}}, c, r) = N_{\text{dof}}(c, r)/W_{\text{total}}(n_{\text{sm}}, c, r)$. Wall times and throughputs are summarized in Table 5. For fixed (ν, n_{sm}, r) , the throughput increases strongly with refinement, reaching the multi- 10^7 dofs/s regime for $r = 2$ at $c = 7$ (and correspondingly high absolute values for $r = 3, 4$). While increasing n_{sm} reduces linear iterations (Table 4), it typically increases wall time (Table 5) because the additional Vanka work dominates the cost per iteration. The dependence on ν is comparatively mild: iteration counts change only marginally (Table 4), and differences in time to solution are primarily attributable to the shifted balance between setup and application cost in the preconditioner (Table 5).

Strong scaling and bottlenecks. Figure 1 shows near-optimal strong scaling for $c = 7$ with $n_{\text{sm}} \in \{1, 2, 4\}$ and $r \in \{2, 3, 4\}$: throughput grows almost linearly with MPI ranks. The runtime breakdown in Figure 2 explains the remaining performance limitations: the Vanka smoother dominates, in particular the costly preconditioner rebuild and the Vanka application, whereas the remainder of the multigrid work becomes comparatively small. Consequently, the iteration reductions obtained by increasing n_{sm} do not translate into shorter time to solution, and the dominance of rebuild/apply becomes more pronounced at higher polynomial degree (Figure 2, Table 5). Overall, the hp STMG method yields robust iteration counts and excellent scalability (Table 4, Figure 1), but the method is expensive due to the computational complexity of the smoother (Figure 2).

6. Conclusions. We presented a monolithic matrix-free hp space-time multigrid method (hp -STMG) for tensor-product space-time finite element discretizations of the incompressible Navier–Stokes equations, based on mapped inf-sup stable pairs

$\mathbb{Q}_{r+1}/\mathbb{P}_r^{\text{disc}}$ in space and $\text{DG}(k)$ in time. Fully coupled nonlinear systems are solved by Newton–GMRES preconditioned with hp -STMG, combining geometric and polynomial coarsening in space and time. The numerical experiments demonstrate robust nonlinear convergence, h - and p -robust Krylov convergence of the hp -STMG preconditioner, and solver performance that remains stable over the investigated range of Reynolds numbers, while achieving near-optimal strong scaling up to $1.843 \cdot 10^4$ MPI ranks and high throughput on problems with more than 10^{12} degrees of freedom.

The performance analysis identifies the dominant bottleneck: the space-time cell-wise Vanka smoother. We proposed an effective approximation via coefficient patch models with single time point evaluation and an inexact application that preserves the robust iteration behavior, yet rebuild and apply remain expensive and dominate time to solution at higher order. The practical results nicely confirm the theory and their outcomes: freezing the coefficients of the nonlinear terms on the local Vanka patch by single time point evaluation introduces a perturbation controlled by the time-step τ , so the inexact patch model remains consistent and improves as $\tau \rightarrow 0$. Tailored temporal quadrature of the nonlinear terms with inexactness for triple products of discrete functions enables efficient time integration, while implying only higher-order quadrature errors. It therefore does not reduce the $\text{DG}(k)$ convergence order. Future work should therefore target cheaper smoothing strategies, for example block-diagonal or approximate factorization variants (e.g. diagonal Vanka [16]), and the incorporation of temporal decoupling ideas into the local space-time systems (e.g. along the lines of [23]), in order to reduce both compute and memory costs without compromising robustness.

Acknowledgments. Computational resources (HPC cluster HSUper) have been provided by the project hpc.bw, funded by dtec.bw - Digitalization and Technology Research Center of the Bundeswehr. dtec.bw is funded by the European Union - NextGenerationEU.

Appendix A. Definition of the assembly matrices and vectors.

Here we summarize the matrices and vectors that are assembled from the bilinear and linear forms in (2.13). This is done for the tensor product spaces in (2.8) and their bases introduced in (3.2) and (3.3), respectively.

Time matrix assembly. For the temporal basis induced by (3.2), we define \mathbf{K}_n^τ , \mathbf{M}_n^τ , $\mathbf{C}_n^\tau \in \mathbb{R}^{k+1, k+1}$ by

$$(A.1a) \quad (\mathbf{K}_n^\tau)_{ab} := \int_{t_{n-1}}^{t_n} \partial_t \varphi_n^b \varphi_n^a dt + \varphi_n^b(t_{n-1}^+) \varphi_n^a(t_{n-1}^+), \quad (\mathbf{M}_n^\tau)_{ab} := \int_{t_{n-1}}^{t_n} \varphi_n^b \varphi_n^a dt,$$

$$(A.1b) \quad (\mathbf{C}_n^\tau)_{ab} := \begin{cases} \varphi_{n-1}^b(t_{n-1}) \varphi_n^a(t_{n-1}^+), & \text{for } n > 1, \\ \varphi_n^a(t_{n-1}^+) \delta_{b,k+1}, & \text{for } n = 1, \end{cases}$$

with the Kronecker symbol $\delta_{\alpha,\beta}$. By the exactness of formula (3.1) for all polynomials of degree less or equal than $2k$, \mathbf{M}_n^τ is diagonal with positive entries $w_{n,\mu} := \frac{\tau_n}{2} \hat{\omega}_\mu$.

Space matrix assembly (bilinear forms). Using the bases in (3.3), we define \mathbf{M}_h , $\mathbf{A}_h \in \mathbb{R}^{M^v \times M^v}$, $\mathbf{B}_h \in \mathbb{R}^{M^p \times M^v}$ and $\mathbf{M}_h^p \in \mathbb{R}^{M^p \times M^p}$ by

$$(A.2a) \quad (\mathbf{M}_h)_{ij} := \int_{\Omega} \chi_j^v \cdot \chi_i^v dx, \quad (\mathbf{A}_h)_{ij} := \int_{\Omega} \nabla \chi_j^v \cdot \nabla \chi_i^v dx,$$

$$(A.2b) \quad (\mathbf{B}_h)_{\ell j} := - \int_{\Omega} (\nabla \cdot \chi_j^v) \chi_\ell^p dx, \quad (\mathbf{M}_h^p)_{\ell m} := \int_{\Omega} \chi_m^p \chi_\ell^p dx.$$

Space matrix assembly (boundary terms). For the bilinear boundary pairings in (2.9) and (2.11), that are due to either the natural boundary conditions arising from

integration by parts or the application of Nitsche's method, we define $\mathbf{G}_{\Gamma_D}^v \in \mathbb{R}^{M^v, M^v}$, $\mathbf{G}_{\Gamma_D}^p \in \mathbb{R}^{M^v, M^p}$, $\mathbf{M}_{\Gamma_D} \in \mathbb{R}^{M^v, M^v}$ and $\mathbf{M}_{\Gamma_D}^n \in \mathbb{R}^{M^v, M^v}$ by

$$(A.3a) \quad (\mathbf{G}_{\Gamma_D}^v)_{ij} := \int_{\Gamma_D} (\partial_n \chi_j^v) \cdot \chi_i^v \, do, \quad (\mathbf{G}_{\Gamma_D}^p)_{ij} := \int_{\Gamma_D} (\chi_j^v \cdot \mathbf{n}) \chi_i^p \, do,$$

$$(A.3b) \quad (\mathbf{M}_{\Gamma_D})_{ij} := \int_{\Gamma_D} \chi_j^v \cdot \chi_i^v \, do, \quad (\mathbf{M}_{\Gamma_D}^n)_{ij} := \int_{\Gamma_D} (\chi_j^v \cdot \mathbf{n}) (\chi_i^v \cdot \mathbf{n}) \, do,$$

and, finally, $\mathbf{N}_{\Gamma_D}^{v,b,r}(\gamma) \in \mathbb{R}^{M^v, M^v}$ by

$$(A.4) \quad \mathbf{N}_{\Gamma_D}^{v,b,r}(\gamma) := -\nu (\mathbf{G}_{\Gamma_D}^v + (\mathbf{G}_{\Gamma_D}^v)^\top) + \nu \frac{\gamma_1}{h_{\Gamma_D}} \mathbf{M}_{\Gamma_D} + \frac{\gamma_2}{h_{\Gamma_D}} \mathbf{M}_{\Gamma_D}^n,$$

Vectors assembly (linear forms). For the linear forms in (2.13) we put

$$(A.5) \quad \mathbf{F}_n := (\mathbf{F}_n^1, \dots, \mathbf{F}_n^{k+1})^\top \in \mathbb{R}^{(k+1) \cdot M^v}, \quad \text{with } (\mathbf{F}_n^a)_i := Q_n(\langle \mathbf{f}, \varphi_n^a \chi_i^v \rangle)$$

for $a = 1, \dots, k+1$ and $n = 1, \dots, N$. Further, we let

$$(A.6) \quad \mathbf{L}_n := (\mathbf{L}_n^1, \dots, \mathbf{L}_n^{k+1})^\top \in \mathbb{R}^{(k+1) \cdot M^v}, \quad \text{with } (\mathbf{L}_n^a)_i := Q_n(B_\gamma(\mathbf{g}, \varphi_n^a \chi_i^v)).$$

In (A.5) and (A.6), we tacitly assume that the data \mathbf{f} and \mathbf{g} are sufficiently smooth in time functions such that their point-wise evaluation in time is well-defined.

Appendix B. Algorithms.

Algorithm 1: Inexact Newton-Krylov (EW + nonmonotone Armijo)

Input: Initial \mathbf{X}_0 , residual $\mathcal{R}(\cdot)$, Jacobian $\mathcal{J}(\cdot)$

Input: Tolerances (abs_{tol} , rel_{tol} , maxit); EW ($\eta_0, c_\eta, \theta, \eta_{\min}, \eta_{\max}$)

Input: Line-search ($\lambda_0, c, \tau, \alpha_{\min}, M$); Rebuild ($\theta_N, \theta_L, \kappa_{\text{abs}}$); Stagn. (s, ϑ)

```

1  $\mathbf{X} \leftarrow \mathbf{X}_0$ ;  $\mathbf{r} \leftarrow \mathcal{R}(\mathbf{X})$ ;  $n_0 \leftarrow \|\mathbf{r}\|_{\mathcal{M}}$ 
2  $n_{\text{prev}} \leftarrow n_0$ ;  $\eta \leftarrow \eta_0$ ;  $\rho_{\text{prev}} \leftarrow 1$ ;  $\kappa_{\text{prev}} \leftarrow 1$ ;  $k \leftarrow 0$ 
3 while  $\|\mathbf{r}\|_{\mathcal{M}} > \text{max}(\text{abs}_{\text{tol}}, \text{rel}_{\text{tol}}, n_0)$  and  $k < \text{maxit}$  do
4   if  $\rho_{\text{prev}} \geq \theta_N$  or  $\kappa_{\text{prev}} \geq \text{max}(\theta_L, \kappa_{\text{ref}}, \kappa_{\text{abs}})$  then
5     | UpdateSmoothenFromMidpoint ( $\mathbf{X}$ );  $\kappa_{\text{ref}} \leftarrow \text{max}(1, \kappa_{\text{prev}})$ 
6     | if  $k > 0$  then  $\eta \leftarrow \text{clamp}\left(c_\eta \eta \left(\|\mathbf{r}\|_{\mathcal{M}} / \text{max}(n_{\text{prev}}, \varepsilon)\right)^\theta, \eta_{\min}, \eta_{\max}\right)$ 
7     |  $(\widehat{\mathbf{X}}, \kappa, \{\rho_j\}) \leftarrow \text{FGMRES}(\mathcal{J}(\mathbf{X}), -\mathbf{r}; \text{tol} = \eta)$  // exact Jacobian
8     |  $\alpha \leftarrow \text{Armijo}(\mathbf{X}, \widehat{\mathbf{X}}, \mathbf{r}, \mathcal{J}(\mathbf{X}); \lambda_0, c, \tau, \alpha_{\min}, M)$ 
9     |  $\mathbf{X} \leftarrow \mathbf{X} + \alpha \widehat{\mathbf{X}}$ 
10    |  $n_{\text{prev}} \leftarrow \|\mathbf{r}\|_{\mathcal{M}}$ ;  $\mathbf{r} \leftarrow \mathcal{R}(\mathbf{X})$ 
11    |  $\rho_{\text{prev}} \leftarrow \|\mathbf{r}\|_{\mathcal{M}} / \text{max}(n_{\text{prev}}, \varepsilon)$ ;  $\kappa_{\text{prev}} \leftarrow \text{max}(1, \kappa)$ 
12    | if Stagnates ( $\{\rho_j\}, s, \vartheta$ ) then UpdateSmoothenFromMidpoint ( $\mathbf{X}$ )
13    |  $k \leftarrow k + 1$ 
14 return  $\mathbf{X}$ 

```

Algorithm 2: Armijo($\mathbf{X}, \widehat{\mathbf{X}}, \mathbf{r}, \mathcal{J}; \lambda_0, c, \tau, \alpha_{\min}, M$)

Input: $\phi(\mathbf{Z}) = \frac{1}{2} \|\mathcal{R}(\mathbf{Z})\|_{\mathcal{M}}^2$; direction $\widehat{\mathbf{X}}$
Output: Step α

- 1 $\alpha \leftarrow \lambda_0$; $\phi_0 \leftarrow \frac{1}{2} \|\mathbf{r}\|_{\mathcal{M}}^2$; $g_0 \leftarrow \mathbf{r}^\top \mathcal{J} \widehat{\mathbf{X}}$
- 2 Initialize nonmonotone window $\mathcal{W} \leftarrow [\phi_0]$ (keep last M) and failures $(\alpha_1, \phi_1), (\alpha_2, \phi_2) \leftarrow \emptyset$
- 3 **while** $\alpha > \alpha_{\min}$ **do**
- 4 $\phi_t \leftarrow \frac{1}{2} \|\mathcal{R}(\mathbf{X} + \alpha \widehat{\mathbf{X}})\|_{\mathcal{M}}^2$; $\phi_{\max} \leftarrow (M > 0) ? \max(\mathcal{W}) : \phi_0$
- 5 **if** $\phi_t \leq \phi_{\max} + c \alpha g_0$ **then**
- 6 **if** $M > 0$ **then** append ϕ_t to \mathcal{W} (keep last M)
- 7 **return** α
- 8 Update $(\alpha_1, \phi_1), (\alpha_2, \phi_2)$ with current fail (α, ϕ_t)
- 9 $\alpha \leftarrow \text{clamp}(\alpha_{\text{interp}}, 0.1\alpha, 0.5\alpha)$; **if** α_{interp} *undefined* **then** $\alpha \leftarrow \tau \alpha$
- 10 **return** α_{\min}

Appendix C. Convergence plots. Figure C.1 shows the convergence in various norms for all polynomial degrees and refinements in Subsection 5.1. The Newton and GMRES iteration counts are given in Table 2.

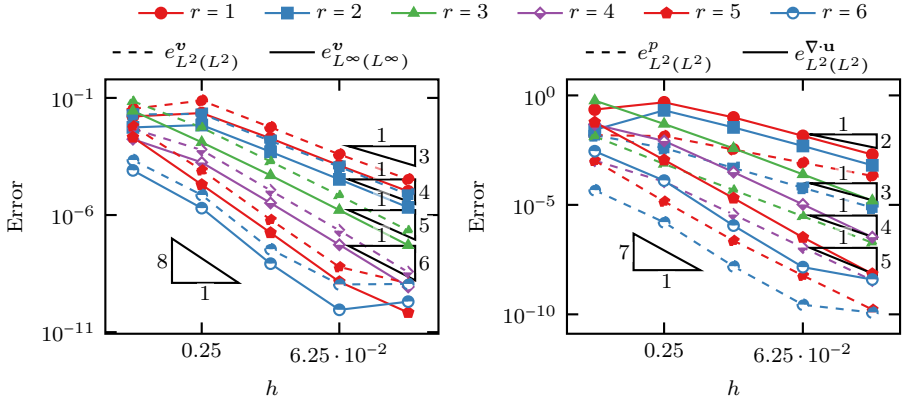


Fig. C.1: Calculated errors of the velocity and pressure in various norms (velocity: L^2 , L^∞ in space-time and the L^2 -norm of the divergence in space-time, pressure: L^2 in space-time) for different polynomial orders. The expected orders of convergence, represented by the triangles, match with the experimental orders.

REFERENCES

- [1] R. ABU-LABDEH, S. MACLACHLAN, AND P. E. FARRELL, *Monolithic multigrid for implicit Runge–Kutta discretizations of incompressible fluid flow*, Journal of Computational Physics, 478 (2023), p. 111961, <https://doi.org/10.1016/j.jcp.2023.111961>.
- [2] P. C. AFRICA, D. ARNDT, W. BANGERTH, B. BLAIS, M. FEHLING, R. GASSMÖLLER, T. HEISTER, L. HELTAI, S. KINNEWIG, M. KRONBICHLER, M. MAIER, P. MUNCH, M. SCHRETER-FLEISCHACKER, J. P. THIELE, B. TURCKSIN, D. WELLS, AND V. YUSHUTIN, *The deal.II library, Version 9.6*, Journal of Numerical Mathematics, 32 (2024), pp. 369–380, <https://doi.org/10.1515/jnma-2024-0137>.

- [3] N. AHMED, C. BARTSCH, V. JOHN, AND U. WILBRANDT, *An Assessment of Some Solvers for Saddle Point Problems Emerging from the Incompressible Navier–Stokes Equations*, Computer Methods in Applied Mechanics and Engineering, 331 (2018), pp. 492–513, <https://doi.org/10.1016/j.cma.2017.12.004>.
- [4] M. ANSELMANN AND M. BAUSE, *A Geometric Multigrid Method for Space-Time Finite Element Discretizations of the Navier–Stokes Equations and its Application to 3D Flow Simulation*, ACM Trans. Math. Softw., 49 (2023), <https://doi.org/10.1145/3582492>.
- [5] M. ANSELMANN, M. BAUSE, N. MARGENBERG, AND P. SHAMKO, *An energy-efficient GMRES–multigrid solver for space-time finite element computation of dynamic poroelasticity*, Computational Mechanics, 74 (2024), pp. 889–912, <https://doi.org/10.1007/s00466-024-02460-w>.
- [6] M. ANSELMANN, M. BAUSE, G. MATTHIES, AND F. SCHIEWECK, *Optimal pressure approximation for the nonstationary Stokes problem by a variational method in time with post-processing*, 2025, <https://arxiv.org/abs/2505.06933>.
- [7] S. C. EISENSTADT AND H. F. WALKER, *Choosing the forcing terms in an inexact Newton method*, SIAM Journal on Scientific Computing, 17 (1996), pp. 16–32, <https://doi.org/10.1137/0917003>.
- [8] L. FAILER AND T. RICHTER, *A Parallel Newton Multigrid Framework for Monolithic Fluid-Structure Interactions*, Journal of Scientific Computing, 82 (2021), <https://doi.org/10.1007/s10915-019-01113-y>.
- [9] N. FEHN, P. MUNCH, W. A. WALL, AND M. KRONBICHLER, *Hybrid Multigrid Methods for High-Order Discontinuous Galerkin Discretizations*, Journal of Computational Physics, 415 (2020), p. 109538, <https://doi.org/10.1016/j.jcp.2020.109538>.
- [10] M. J. GANDER AND T. LUNET, *Time Parallel Time Integration*, Society for Industrial and Applied Mathematics, Philadelphia, PA, 2024, <https://doi.org/10.1137/1.9781611978025>.
- [11] L. GRIPPO, F. LAMPARIELLO, AND S. LUCIDI, *A nonmonotone line search technique for newton’s method*, SIAM Journal on Numerical Analysis, 23 (1986), pp. 707–716, <https://doi.org/10.1137/0723046>.
- [12] J. G. HEYWOOD AND R. RANNACHER, *Finite element approximation of the nonstationary navier–stokes problem. i. regularity of solutions and second-order error estimates for spatial discretization*, SIAM Journal on Numerical Analysis, 19 (1982), pp. 275–311, <https://doi.org/10.1137/0719018>.
- [13] J. G. HEYWOOD AND R. RANNACHER, *Finite-element approximation of the nonstationary navier–stokes problem. part iv: Error analysis for second-order time discretization*, SIAM Journal on Numerical Analysis, 27 (1990), pp. 353–384, <https://doi.org/10.1137/0727022>.
- [14] D. JODELAUER, U. LANGER, T. WICK, AND W. ZULEHNER, *Matrix-Free Monolithic Multigrid Methods for Stokes and Generalized Stokes Problems*, SIAM Journal on Scientific Computing, 46 (2024), pp. A1599–A1627, <https://doi.org/10.1137/22M1504184>.
- [15] V. JOHN, *Finite Element Methods for Incompressible Flow Problems*, vol. 51 of Springer Series in Computational Mathematics, Springer, 2016, <https://doi.org/10.1007/978-3-319-45750-5>.
- [16] V. JOHN AND L. TOBISKA, *Numerical performance of smoothers in coupled multigrid methods for the parallel solution of the incompressible Navier–Stokes equations*, International Journal for Numerical Methods in Fluids, 33 (2000), pp. 453–473, [https://doi.org/10.1002/1097-0363\(20000630\)33:4<453::AID-FLD15>3.0.CO;2-0](https://doi.org/10.1002/1097-0363(20000630)33:4<453::AID-FLD15>3.0.CO;2-0).
- [17] O. KARAKASHIAN AND C. MAKRIDAKIS, *Convergence of a continuous galerkin method with mesh modification for nonlinear wave equations*, Mathematics of Computation, 74 (2005), pp. 85–102, <https://doi.org/10.1090/S0025-5718-04-01654-0>.
- [18] N. KOHL AND U. RÜDE, *Textbook Efficiency: Massively Parallel Matrix-Free Multigrid for the Stokes System*, SIAM Journal on Scientific Computing, 44 (2022), pp. C124–C155, <https://doi.org/10.1137/20M1376005>.
- [19] M. KRONBICHLER AND K. KORMANN, *A Generic Interface for Parallel Cell-Based Finite Element Operator Application*, Computers & Fluids, 63 (2012), pp. 135–147, <https://doi.org/10.1016/j.compfluid.2012.04.012>.
- [20] N. MARGENBERG, *A Monolithic HP Space-Time Multigrid Preconditioned Newton-Krylov Solver for Space-Time FEM Applied to the Incompressible Navier-Stokes Equations*, 2026, <https://doi.org/10.5281/zenodo.18641316>.
- [21] N. MARGENBERG, M. BAUSE, AND P. MUNCH, *An hp multigrid approach for tensor-product space-time finite element discretizations of the stokes equations*, SIAM Journal on Scientific Computing, 47 (2025), pp. B1503–B1529, <https://doi.org/10.1137/25M1734142>.
- [22] N. MARGENBERG AND P. MUNCH, *A Space-Time Multigrid Method for Space-Time Finite Element Discretizations of Parabolic and Hyperbolic PDEs*. arXiv preprint, 2024, <https://arxiv.org/abs/2401.01234>.

//doi.org/10.48550/arXiv.2408.04372.

[23] P. MUNCH, I. DRAVINS, M. KRONBICHLER, AND M. NEYTCHEVA, *Stage-Parallel Fully Implicit Runge–Kutta Implementations with Optimal Multilevel Preconditioners at the Scaling Limit*, SIAM Journal on Scientific Computing, (2023), pp. S71–S96, <https://doi.org/10.1137/22M1503270>.

[24] P. MUNCH, T. HEISTER, L. PRIETO SAAVEDRA, AND M. KRONBICHLER, *Efficient Distributed Matrix-free Multigrid Methods on Locally Refined Meshes for FEM Computations*, ACM Transactions on Parallel Computing, 10 (2023), pp. 3:1–3:38, <https://doi.org/10.1145/3580314>.

[25] W. PAZNER AND P.-O. PERSSON, *Stage-parallel fully implicit runge–kutta solvers for discontinuous galerkin fluid simulations*, Journal of Computational Physics, 335 (2017), pp. 700–717, <https://doi.org/10.1016/j.jcp.2017.01.050>.

[26] R. PICARD AND D. MCGHEE, *Partial Differential Equations: A unified Hilbert Space Approach*, De Gruyter, 2011, <https://doi.org/10.1515/9783110250275>.

[27] L. PRIETO SAAVEDRA, P. MUNCH, AND B. BLAIS, *A matrix-free stabilized solver for the incompressible Navier–Stokes equations*, Journal of Computational Physics, 538 (2025), p. 114186, <https://doi.org/10.1016/j.jcp.2025.114186>.

[28] S. RHEBERGEN, B. COCKBURN, AND J. J. W. VAN DER VEGT, *A space-time discontinuous galerkin method for the incompressible navier–stokes equations*, Journal of Computational Physics, 233 (2013), pp. 339–358, <https://doi.org/10.1016/j.jcp.2012.08.052>.

[29] J. ROTH, J. P. THIELE, U. KÖCHER, AND T. WICK, *Tensor-Product Space-Time Goal-Oriented Error Control and Adaptivity With Partition-of-Unity Dual-Weighted Residuals for Nonstationary Flow Problems*, Computational Methods in Applied Mathematics, (2023), <https://doi.org/10.1515/cmam-2022-0200>.

[30] Y. SAAD, *A flexible inner-outer preconditioned gmres algorithm*, SIAM Journal on Scientific Computing, 14 (1993), pp. 461–469, <https://doi.org/10.1137/0914028>.

[31] B. S. SOUTHWORTH, O. KRZYSIK, AND W. PAZNER, *Fast solution of fully implicit runge–kutta and discontinuous galerkin in time for numerical pdes, part ii: Nonlinearities and daes*, SIAM Journal on Scientific Computing, 44 (2022), pp. A636–A663, <https://doi.org/10.1137/21M1390438>.

[32] S. P. VANKA, *Block-Implicit Multigrid Solution of Navier–Stokes Equations in Primitive Variables*, J. Comp. Phy., 65 (1985), pp. 138–158, [https://doi.org/10.1016/0021-9991\(86\)90008-2](https://doi.org/10.1016/0021-9991(86)90008-2).

[33] A. VORONIN, G. HARPER, S. MACLACHLAN, L. N. OLSON, AND R. S. TUMINARO, *Monolithic multigrid preconditioners for high-order discretizations of stokes equations*, 2025, <https://doi.org/10.1137/24M1675588>.

[34] H. WOBKER AND S. TUREK, *Numerical Studies of Vanka-Type Smoothers in Computational Solid Mechanics*, Adv. Appl. Math. Mech., (2009).